Visualizing looping of two endogenous genomic loci using synthetic zinc-finger proteins with anti-FLAG and anti-HA frankenbodies in living cells

Yang Liu[1, #], Ning Zhao[2, #], Masato T. Kanemaki[3, 4], Yotaro Yamamoto[5], Yoshifusa Sadamura[5], Timothy J. Stasevich[2, 6, *], Hiroshi Kimura[1, 6, *]

[1] School of Life Science and Technology, Tokyo Institute of Technology, Yokohama, 226-8501, Japan
[2] Department of Biochemistry and Molecular Biology, Colorado State University, Fort Collins, CO, USA
[3] Department of Chromosome Science, National Institute of Genetics, Research Organization of Information and Systems, Mishima, Shizuoka 411-8540, Japan
[4] Department of Genetics, SOKENDAI, Mishima, Shizuoka 411-8540, Japan
[5] Life Science Research Laboratories, Fujifilm Wako Pure Chemical, Amagasaki, 661-0963, Japan
[6] Cell Biology Center and World Research Hub Initiative, Tokyo Institute of Technology, Yokohama, 226-8503, Japan

* To whom correspondence should be addressed.
Hiroshi kimura, Tel: +81-45-924-5742; Email: hkimura@bio.titech.ac.jp

* Correspondence may also be addressed to:
Timothy J. Stasevich, Tel: +1-970-491-0583; Email: Tim.Stasevich@colostate.edu

[#] The authors wish it to be known that, in their opinion, the first two authors should be regarded as joint First Authors.

ABSTRACT

In eukaryotic nuclei, chromatin loops mediated through cohesin are critical structures that regulate gene expression and DNA replication. Here we demonstrate a new method to visualize endogenous genomic loci using synthetic zinc-finger proteins harboring repeat epitope tags (ZF probes) for signal amplification via binding of tag-specific intracellular antibodies, or frankenbodies, fused with fluorescent proteins. We achieve this in two steps. First, we develop an anti-FLAG frankenbody that can bind FLAG-tagged proteins in diverse live-cell environments. The anti-FLAG frankenbody complements the anti-HA frankenbody, enabling two-color signal amplification from FLAG and HA-tagged proteins. Second, we develop a pair of cell-permeable ZF probes that specifically bind two endogenous chromatin loci predicted to be involved in chromatin looping. By coupling our anti-FLAG and anti-HA frankenbodies with FLAG- and HA-tagged ZF probes, we simultaneously visualize the dynamics of the two loci in single living cells. This reveals close association between the two loci in the majority of cells, but the loci markedly separate upon the triggered degradation of the cohesin subunit RAD21. Our ability to image two endogenous genomic loci simultaneously in single living cells provides a proof-of-principle that ZF probes coupled with frankenbodies are useful new tools for exploring genome dynamics in multiple colors.

INTRODUCTION

During cell cycle progression and cell differentiation, chromosomes undergo dynamic changes in their structure and organization. In the interphase nucleus, for example, chromatin loops are critical structures that regulate gene expression and DNA replication (1, 2). Chromosome conformation capture (3C, 3) and Hi-C (4) analyses have revealed chromatin loops help separate active chromatin domains from inactive ones (5). The formation of chromatin loops creates chromosome clusters, also known as chromosome compartments, that span several hundred Kb to a few Mb (6, 7), contain topologically associating domains (TADs), CTCF (CCCTC-binding factor) binding sites, and cohesin complexes (8).

So far, chromatin looping has mainly been investigated in fixed cells using Hi-C (6, 7) and fluorescence in situ hybridization (FISH; 9-13). While powerful, these assays require fixation, leaving the dynamics of chromatin looping unclear. To better resolve these dynamics, a sequence-specific live-cell imaging technology would be useful (14).

To image genomic loci in living cells, several methods have been developed. The pioneering work labeled specific or non-specific genomic loci by inserting tens or hundreds of lac or tet operators that could be bound by fluorescent Lac or Tet repressors. This created ultra-bright fluorescent spots that marked the location of the repeats within the genome so they could be tracked for long periods of time using standard fluorescence microscopy (15, 16). Such artificial repeat-based methods can yield high contrast images because hundreds of fluorophores can be present in a single spot. In this approach, however, extensive genomic manipulation is essential and the insertion may affect gene regulation around the inserted locus. Recently, endogenous loci have been visualized using zinc-finger (ZF) proteins, transcription activator-like effectors (TALEs), and CRISPR/nuclease-deficient Cas9 (dCas9) systems (17-20). Whereas most probes target repeat sequences, specific genomic loci can also be labeled with multiple unique probes (21). CRISPR/dCas9 has been a convenient and popular method because probe specificity is easily modulated by altering sgRNA sequence, whereas it is essential to design and construct zinc-finger proteins and TALEs for each specific sequence. However, the strong DNA-binding nature of some probes, including Lac repressor and dCas9 with sgRNA, could interfere with DNA replication, repair and transcription (22). By contrast, ParB and ZF proteins have been shown to interfere less with such events (23-25).

In this study, we develop an orthogonal technology for genome visualization based on ZF DNA-binding proteins harboring repeat epitope tags for signal amplification by epitope-specific intracellular antibodies. To achieve this, we first developed an anti-FLAG “frankenbody” – a chimeric single chain variable fragment that binds FLAG epitopes in living cells – to complement our recently developed anti-HA frankenbody (26). Together, these two frankenbodies can bind and label HA- and FLAG-tagged proteins with two distinct fluorophores in single living cells. We next generated a pair of cell-permeable ZF DNA-binding probes (27-29) and tagged them with 10× HA or FLAG epitopes. When these primary ZF probes are delivered into living cells that express anti-HA and anti-FLAG frankenbodies with different fluorescent proteins as secondary probes, two distinct endogenous genomic loci can be simultaneously marked and tracked. Using this system, we followed two genomic regions that are near cohesin binding sites and show close contact in cellular 3D space according to

HiC. Upon triggered cohesin degradation (30), the two regions became more separated, confirming that the strategy can be used to monitor cohesin-mediated chromatin contacts. We anticipate our ZF-based technology can now be extended to monitor other endogenous genomic loci and investigate the dynamics of higher-order chromatin structures in a multiplexed manner.

MATERIAL AND METHODS

Construction of plasmids for anti-FLAG frankenbody development and characterization

Variable regions of antibody heavy and light chains encoding an anti-FLAG antibody were amplified by PCR and the nucleotide sequences were determined (31). Wildtype and chimeric anti-FLAG scFv genes were synthesized as gblocks. The scFv gblocks were ligated with linearized anti-HA frankenbody-mEGFP (Addgene # 129590) by EcoRI through Gibson assembly (anti-FLAG FB-mEGFP). Anti-FLAG frankenbody fused with mRuby2 was constructed by Gibson assembly by ligating NotI-linearized anti-FLAG FB-mEGFP with mRuby2 amplified from a previously built plasmid (4×HA-mRuby-Kv2.1). Anti-FLAG frankenbody fused with SNAP-tag and HaloTag plasmids were constructed by ligating previously built plasmids, anti-HA FB-SNAP and anti-HA FB-Halo (Addgene #129592), cut by EcoRI and combined with anti-FLAG frankenbody gblocks by Gibson assembly.

4×FLAG-mCh-H2B and 4×FLAG-mCh-β-actin plasmids were built by Gibson assembly by ligating a synthesized 4×FLAG gblock with previously built 1×HA-mCh-H2B or 1×HA-mCh-β-actin plasmids cut by AgeI and NotI. 4×FLAG-sfGFP-H2B was built by ligating 4×FLAG-mCh-H2B cut by NotI and BglII with sfGFP-H2B amplified from an Addgene plasmid, sfGFP-H2B-C-10 (#56367). Mito-mCh-1×FLAG and Mito-mCh-smFLAG were constructed by ligating 1×FLAG synthesized by overlapping PCR and smFLAG amplified from smFLAG-KDM5B-24×MS2 with previously built Mito-mCh-1×HA cut by BglII and BamHI through Gibson Assembly.

The gblocks were synthesized by Integrated DNA Technologies and the recombinant plasmids were sequence verified by Quintara Biosciences. All plasmids used for imaging were prepared using a NucleoBond Xtra Midi EF kit (Macherey-Nagel) with a final concentration of about 1 mg/mL. All the detailed sequence information is available upon request and the final anti-FLAG frankenbody expression constructs will be deposited to Addgene.

Cell culture and transfection

U2OS cells (ATCC HTB-96) were cultured in DMEM medium (Thermo Fisher Scientific) supplemented with 10% (v/v) fetal bovine serum (FBS; Altas Biologicals), 1 mM L-glutamine and 1% (v/v) penicillin-streptomycin (Thermo Fisher Scientific) at 37°C, in a cell culture incubator under 5% of CO_2. HCT116-RAD21-mAID-mClover cells (30) were cultured in McCoy's 5A (Modified) Medium with 10% FBS (Thermo Fisher Scientific) and 1% Glutamine-Penicillin-Streptomycin solution (Sigma-Aldrich) at 37°C in a cell culture incubator under 5% of CO_2. HCT116 (ATCC), HEK-293T (obtained from Kei Fujinaga at Sapporo Medical School in 1980s) and A9 cells (obtained from Nobuo Takagi at Hokkaido University in 1980s) were cultured in DMEM (Nacalai Tesque) with 10% FCS (Thermo Fisher Scientific) and 1% GPS solution (Sigma-Aldrich) at 37°C in a cell culture incubator under 5% of

CO_2. Lipofectamine LTX reagent with PLUS reagent (Thermo Fisher Scientific) or Lipofectamine 3000 (Thermo Fisher Scientific) was used for transfection following the manufacturer's instructions.

Preparing cells for imaging single-mRNA translation dynamics

Imaging reagents (smFLAG-KDM5B-24×MS2/anti-FLAG FB-GFP and purified MCP-HaloTag protein) needed for nascent chain tracking and puromycin treatment were bead loaded into cells as previously described (26). Briefly, U2OS cells were plated on 35 mm MatTek chambers (MatTek) the day before imaging. On the imaging day, the medium in the MatTek chambers was changed to Opti-MEM (Thermo Fisher Scientific) with 10% FBS. The cells were incubated in the Opti-MEM for 20 min. Then 4 µL of a mixture of plasmids (1 µg of smFLAG-KDM5B-24×MS2 and 0.5 µg of anti-FLAG FB-GFP) and purified MCP-HaloTag (130 ng) in PBS was pipetted on top of the cells after removing the Opti-medium from the MatTek chamber, and ~106 µm glass beads (Sigma Aldrich) were evenly distributed on top. The chamber was then tapped firmly seven times, and Opti-medium was added back to the cells (32). 3 h post bead loading, the cells were stained in 1 mL of 0.2 µM of JF646-HaloTag ligand (33) diluted in phenol-red-free complete DMEM. After 20 min of staining, the cells were washed three times in phenol-red-free complete DMEM to remove glass beads and excess dyes. The cells were then ready for imaging.

Fluorescence recovery after photobleaching experiments

Fluorescence recovery after photobleaching (FRAP) assays were performed on cells transiently transfected with 4×FLAG-mCh-H2B and anti-FLAG FB-mEGFP 18~22 h before FRAP. The images were acquired using an Olympus IX81 spinning disk confocal (CSU22 head) microscope coupled to a Phasor photomanipulation unit (Intelligent Imaging Innovations) with a 100×oil immersion objective (NA 1.40). Before photobleaching, 20 frames were acquired with a 1s time interval. The images were captured using a 488 nm laser (0.77 mW) followed by a 561 nm (0.42 mW) laser. The laser exposure time was adjusted according to the fluorescence intensity. The spinning disk was set up at a 1 × 1 spin rate. Images were acquired with a Photometrics Cascade II EM-CCD camera using SlideBook software (Intelligent Imaging Innovations). After acquiring pre-FRAP images, the 488 nm laser (from the Phasor unit for photobleaching) was set to 17 mW with a 100 ms exposure time to photobleach a circular region in the nucleus. After photobleaching, 30 images were captured without delay, and then an additional 100 images were acquired with a 5s delay using the same imaging settings as the pre-FRAP images. The fluorescence intensity through time of the photobleached spot was exported using Slidebook software (Intelligent Imaging Innovations). The fluorescence intensity of the nucleus and background were obtained by ImageJ. The FRAP curve and thalf were obtained using easyFRAP-web (34), according to the website instructions.

Imaging conditions for FLAG colocalization experiments and nascent chain tracking

For the co-localization assays in Figs. 1b, 1d and 2a, images were acquired using an Olympus IX81 spinning disk confocal (CSU22 head) microscope using a 100× oil immersion objective (NA 1.40) under the following conditions: 488 nm (0.77 mW) and 561 nm (0.42 mW) sequential imaging for 50

time points without delay at a single plane for Figs. 1b and 1d, and for five time points without delay with 13 z-slices to cover the whole cell body for each time point for Fig. 2a; 1 × 1 spin rate, exposure time adjusted by cell brightness. Images were acquired with a Photometrics Cascade II EM-CCD camera using SlideBook software (Intelligent Imaging Innovations). The displayed images in Figs. 1b and 1d were generated by averaging 50 time points and the images in Fig. 2a were generated by averaging five time points and then max-projecting all z-slices in ImageJ.

For tracking nascent chains with anti-FLAG frankenbody, a custom-built widefield fluorescence microscope based on an inclined illumination (HILO) scheme (35) was used. Briefly, the excitation beams, 488, 561, 637 nm solid-state lasers (Vortran), were coupled and focused off-axis on the rear focal plane of the objective lens (APON 60× TIRF, NA 1.49; Olympus). The emission signals were split by an imaging grade, ultra-flat dichroic mirror (T660lpxr, Chroma). The longer emission signals (far-red) after splitting were passed through a bandpass filter (FF01-731/137-25, Semrock). The shorter emission signals (red and green) after splitting were passed through either a bandpass filter for red (FF01-593/46-25, Semrock) or a bandpass filter for green (FF01-510/42-25, Semrock) installed in a filter wheel (HS-625 HSFW TTL, Finger Lakes Instrumentation). The longer (far-red) and the shorter (red and green) emission signals were detected by two separate EM-CCD cameras (iXon Ultra 888, Andor) by focusing with 300 mm achromatic doublet lenses (AC254-300-A-ML, Thorlabs). The combination of the 60× objective lens from Olympus, a 300 mm tube lens, and iXon Ultra 888 produces 100× images with 130 nm pixel−1. A stage top incubator for temperature (37 °C), humidity, and 5% CO_2 (Okolab) is equipped on a piezoelectric stage (PZU-2150, Applied Scientific Instrumentation) for live cell imaging. The lasers, the cameras, the piezoelectric stage, and the filter wheel were synchronized by an open source microcontroller, Arduino Mega board (Arduino). Imaging acquisition was performed using open source Micro-Manager software (1.4.22).

The imaging size was set to the center 512 × 512 pixels2 (66.6 × 66.6 μm2), and the camera integration time was set to 53.64 ms. The readout time of the cameras from the combination of our imaging size, readout mode (30 MHz), and vertical shift speed (1.13 μs) was 23.36 ms, resulting in an imaging rate of 13 Hz (70 ms per image). Red and green signals were imaged alternatively. The emission filter position was changed during the camera readout time. To minimize the bleed-through, the far-red signal was simultaneously imaged with the green signal. To capture the whole thickness of the cytoplasm in cells, 13 z-stacks with a step size of 0.5 μm (6 μm in total) were imaged. For Fig. 2c, cells were imaged using the above described microscope setup with a 4 s interval between frames (lasers: 488 nm, 13 μW; 637 nm, 150 μW; Laser powers were measured at the back-focal plane of the objective). The displayed image was max-projected through the whole cell volume in ImageJ.

For puromycin treatments, U2OS cells seeded on 35mm MatTek chambers with 70% confluency were loaded with 1 μg of smFLAG-KDM5B-24×MS2 (Addgene #81084), 0.5 μg of anti-FLAG FB-GFP and 130 ng of purified MCP-HaloTag protein by bead loading (32). 3 h post bead loading, imaging chambers were stained and washed as described above. The cells showing translation spots and mRNA molecules were imaged with 20 s intervals between each time point. At each time point, 13 z-slices were imaged with 0.5 μm step size. After acquiring 5 time points as pre-treated images, puromycin was added to imaging chambers at a final concentration of 0.1 mg/mL. After adding

puromycin, the cells were continuously imaged at the same conditions until the translation spots disappeared.

ZF probes design, construction and purification

The ZF probes were designed to target a pair of chromatin contact sites on chromosome 8 (chr8:126, 150, 000-126, 750, 000). Each ZF probe contains 6 zinc finger DNA binding domains engineered using Zinc Finger Tools (37). In this study, the ZF probes were fused with 10× HA or FLAG epitopes at the C-terminus with a linker sequence (GSAGSAAGSGEF; 36). The DNA encoding ZF probes were cloned into the pTrcHis vector (Thermo Fisher Scientific) and verified by nucleotide sequencing. All the detailed sequence information is available upon request and the final ZF probe expression constructs will be deposited to Addgene. Then the sequence-confirmed pTrcHis-ZF vectors were transformed into BL21(DE3) (Sigma). Single colonies were picked up and cultured overnight in LB medium containing 100 μg/mL ampicillin. The culture was diluted 1:500 in 500 ml LB containing 100 μg/mL ampicillin and incubated at 37°C until OD600 reached ~0.6. After the addition of IPTG (Isopropyl β-D-1 thiogalactopyranoside; Sigma; 2 mM) and $ZnCl_2$ (100 μM), cells were regrown overnight at 16°C. After harvesting cells by centrifugation at 4000×g for 30 min at 4°C, the pellets were washed and resuspended in 5 mL lysis buffer (50 mM NaH_2PO_4, 200 mM NaCl, 10 mM imidazole, pH 8.0) with protease inhibitor cocktail (Nacalai Tesque). The cells were lysed by sonicating with 50% power setting for 15 min (15 s on/off) in ice water. After the centrifugation at 15, 000×g for 30 min at 4°C, the supernatant was collected, filtered through a 0.45 μm filter, and applied to a 1 mL HisTrap HP column (GE Healthcare) using an AKAT Prime Plus (GE Healthcare) according to the programmed His-tag elution method: equilibration with 5× column volume lysis buffer, washing with 10× column volume wash buffer (50 mM NaH_2PO4, 200 mM NaCl, 100 mM imidazole, pH 8.0), eluting with 4 mL 0 to 100% gradient with elution buffer (50 mM NaH_2PO4, 200 mM NaCl, 500 mM imidazole, pH 8.0), and 20 mL elution buffer.

Electrophoretic mobility shift assays

Cy3-labeled 36 nt long single-stranded oligonucleotides which contains ZF probe target sites were mixed with the unlabeled complementary oligonucleotides in TE buffer (10 mM Tris-HCl, pH 7.5, 1 mM EDTA), heated to 95°C for 5 min and cooled down at room temperature. The binding reactions were carried out in a 20 μL system (10 mM Tris-HCl, pH 7.5, 50 mM KCl, 5 mM $MgCl_2$, 100 μM $ZnCl_2$, 1 mM dithiothreitol (DTT), 0.05% Triton X-100, and 2.5% glycerol) with various concentration of ZF probes and fixed 20 nM labeled double-stranded oligonucleotides. The binding reaction were incubated at 37°C for 30 min and separated on 8% polyacrylamide gels (FUJIFILM Wako Pure Chemical) in 1×TBE buffer (89 mM Tris, 89 mM boric acid, 2 mM EDTA) at room temperature for 1 h. The fluorescence images were captured using a gel documentation system (LuminoGraph II, ATTO). The KD for ZF probe was calculated using the adapted Michaelis-Menten equation:

$$\text{Fraction bound} = V_{max} * ([\text{ZF probe}] / (K_D + [\text{ZF probe}])) \quad (1)$$

Fraction bound is the ratio of bound signal to the total signal (bound + unbound signal) measured by ImageJ. Vmax and KD were obtained by performing non-linear regression using the adapted Michaelis-Menten equation by JASP ver 0.14.1 (JASP Team; https://jasp-stats.org/).

Live cell imaging of ZF probes

Cells were plated on a 35 mm glass-bottom dish (AGT Technology Solutions) at least a day before imaging. The medium was replaced to FluoroBrite DMEM (Thermo Fisher Scientific) containing 10% FCS and 1% GPS solution (Sigma-Aldrich) after ZF probe administration. Fluorescent images were acquired using a spinning disk confocal microscope (Ti-E, Nikon; CSU-W1, Yokogawa Electric) equipped with a stage incubator at 37°C with 5% CO_2 (Tokai Hit) with an EM-CCD (iXon2; Andor) and a laser system (488, 561, and 640 nm lasers; LNU-4; Nikon) using NIS-Elements ver 4.30 operation software (Nikon). The RAD21-GFP capture was set up as 400 ms exposure time under 75% laser transmission with 11 z-stacks (0.2 um each). The mCherry and iRFP capture setup was adjusted based on the cell condition, typically setup as 400 to 600 ms exposure time under 100% laser transmission with 11 to 15 z-stacks (0.2 um each).

Image analysis and processing were performed using ImageJ2 (38). To measure the distance between the two ZF probes, their focus areas were first defined by thresholding and then distances between the surface pixels of the two foci were measured in all combinations. The average distance of the minimum and maximum distances was calculated and used as the distance between the two foci. For Fig.6A, the area of the nucleus was selected manually by visual inspection to measure RAD21-mAID-mClover-GFP signals. Statistical analyses were performed using JASP ver 0.14.1 (JASP Team; https://jasp-stats.org/). Plots were generated using the plotly package (Plotly Technologies Inc.; https://plot.ly) in the R language (R Core Team; https://www.R-project.org/). Outliers were defined as points above or below 1.5 times the interquartile range from the 25th and 75th percentile. Fig. 3 was created using BioRender.com with a student plan subscription.

Lentivirus-mediated knockdown by shRNA expression

The addgene pLKO.1 lentiviral knockdown protocol was adapted. Gene-specific shRNA and scrambled shRNA were designed using the TRC shRNA Design online tool on GPP Web Portal (https://portals.broadinstitute.org/gpp/public/; 39; Supplementary Table S1). HEK-293T cells were grown up to ~80% confluency in a 6 cm culture dish and were transfected with psPAX2, pCMV-VSV-G, and pLKO.1 puro-based plasmid harboring the designed shRNA (pCMV-VSV-G and pLKO.1 puro were a gift from Bob Weinberg, Addgene plasmid #8454; http://n2t.net/addgene:8454; RRID: Addgene_8454; psPAX2 was a gift from Didier Trono, Addgene plasmid #12260; http://n2t.net/addgene:12260; RRID: Addgene_12260) using Lipofectamine 3000 (Thermo Fisher Scientific) following the manufacturer's instructions. One day after the transfection, the medium was replaced with 5 mL fresh DMEM, which was harvested the next day. The harvested medium (6 mL) was filtered through a 0.2 μm filter and added to HCT116 cells at ~70% confluent in a 6 cm dish (5 mL) with 8 μg/mL polybrene. After an incubation period of 24 h, the medium was replaced to fresh DMEM with 2 μg/mL puromycin for at least 3 days to select infected cells before analysis.

The efficiency of shRNA-mediated knockdown was assessed by immunoblotting. Cells were washed with ice-cold PBS twice and lysed by RIPA buffer (50 mM Tris-HCl, pH 8.0, with 150 mM sodium chloride, 1.0% Igepal CA-630 (NP-40), 0.5% sodium deoxycholate, and 0.1% sodium dodecyl sulfate) at 1 x 10^7/ml. After denaturation by heating at 95°C for 10 min, the protein concentration was measured using a bicinchoninic acid assay kit (FUJIFILM Wako Pure Chemical) and adjusted to 2 mg/mL. Cell lysates (10 µg each) were separated on 7.5% polyacrylamide gels and transferred on to PVDF membranes (Pall). Then the membranes were incubated in Blocking One (Nacalai Tesque) for 30 min, incubated with the primary antibody in Can Get Signal Solution I (TOYOBO) overnight at 4°C with gentle shaking, washed in TBS-T (20 mM Tris-HCl, pH 8.0, 150 mM NaCl, 0.05% Tween 20) for 10 min three times, and incubated with the secondary antibody for 1 h at room temperature in Can Get Signal Solution II (TOYOBO). After washing with TBS-T for 10 min three times, the membranes were incubated with ImmunoStar LD (FUJIFILM Wako Pure Chemical) for 5 min before detecting the chemiluminescent signals using a LuminoGraph II gel documentation system (ATTO).

RESULTS

Development and evaluation of an anti-FLAG frankenbody to image FLAG epitopes in living cells

To label and track a pair of endogenous genomic loci in single living cells with minimal perturbation, we envisioned developing a pair of complementary ZF-based probes, the first harboring a 10× HA tag and the second a 10× FLAG tag for signal amplification in two separate colors. To amplify signals at the 10× HA tag, we recently developed a chimeric anti-HA single-chain variable fragment (scFv), which we refer to as the anti-HA “frankenbody” (26). To similarly amplify signals at the 10× FLAG tag, we set out to develop a complementary anti-FLAG frankenbody (Fig. 1A; Supplementary Fig. 1A).

We began with an anti-FLAG scFv generated from a monoclonal antibody against the DYKDDDDK tag. Unfortunately, this wild-type anti-FLAG scFv (wtFLAG-scFv) did not show any binding affinity to the FLAG tag in living U2OS cells. In particular, a GFP-tagged version of the wtFLAG-scFv did not colocalize in the cell nucleus with a FLAG-tagged mCherry-H2B (Supplementary Fig. 1B and 1C). We hypothesized that the loss of binding affinity is due to misfolding of the scFv. This is a common issue for scFvs since their heavy and light chains are fused in an unnatural way and their disulfide bonds are reduced in the cytoplasm of living cells (26, 40).

To overcome these issues, we engineered more soluble chimeric scFv frankenbodies by grafting all six complementary determining regions (CDRs) or loops of the wtFLAG-scFv to scFv scaffolds that have already been demonstrated to fold correctly in living cells (Fig. 1A; Supplementary Fig. 1A). We chose five scFv scaffolds as loop-grafting candidates: 1) an scFv that binds to histone H4 mono-methylated at Lysine 20 (H4K20me; 15F11; 41); 2) an H4K20me2-specific scFv (2E2; 26); 3) an H3K9ac-specific scFv (13C7; 31); 4) a Suntag-specific scFv (42); and 5) a bone Gla protein (BGP)-specific scFv (KTM219) (43). Among these five scFv scaffolds, their sequence identity with wtFLAG-scFv ranged from 43-74% for the variable region of the heavy chain (VH) and from 58-82% for the variable region of light chain (VL), as shown in Supplementary Table S2.

In general, the higher the sequence identity in the VH and VL regions, the more likely loop grafting will be successful (26, 40). Among the five selected scFv scaffold candidates, 15F11 and 2E2 share the highest sequence identity with wtFLAG-scFv. We therefore predicted that grafting onto the 15F11 and 2E2 scaffolds would have a higher chance of producing a functional anti-FLAG frankenbody. As shown in Supplementary Fig. 1D and 1F, this was indeed the case. In particular, GFP-tagged frankenbodies generated by loop grafting onto the 15F11 and 2E2 scaffolds showed excellent colocalization in the nucleus with FLAG-tagged mCherry-H2B, while the other frankenbodies did not colocalize in the nucleus. Moreover, in the absence of FLAG tags, the 15F11 and 2E2 anti-FLAG frankenbodies were evenly spread throughout cells (Supplementary Fig. 1E and 1F), demonstrating these frankenbodies do not have any off-target binding sites. Together, these two anti-FLAG frankenbodies complement our previously engineered anti-HA frankenbodies (26), demonstrating the power of one-step loop grafting for generating functional intrabodies against linear epitope tags in a fast manner.

To further characterize the 15F11 anti-FLAG frankenbody, we imaged it in diverse live-cell environments. For this, we co-transfected the monomeric enhanced GFP-tagged frankenbody (anti-FLAG FB-mEGFP) with plasmids encoding various FLAG-tagged proteins, including the nuclear protein H2B (4×FLAG-mCh-H2B, also used in the initial screen in Supplementary Fig. 1D), the cytoplasmic protein β-actin (4×FLAG-mCh-β-actin), and the mitochondrial protein mitoNEET (Mito-mCh-1×FLAG; 44). In all cases, the anti-FLAG FB-mEGFP was highly co-localized with the FLAG-tagged proteins (Fig. 1B). In particular, plots of the fluorescence in the two channels along lines spanning each cell revealed high correlations with Pearson correlation coefficients all greater than 0.98 (Fig. 1C). These data demonstrate that the anti-FLAG frankenbody can bind specifically to the FLAG tag fused to both the N- and C-terminal ends of proteins in diverse cellular settings.

We next characterized the functionality of the anti-FLAG frankenbody when fused to different fluorescent proteins beyond mEGFP, including mRuby2, mCherry, SNAP-tag, and HaloTag. To do this, we co-transfected into U2OS cells a plasmid encoding the anti-FLAG frankenbody fused to each fluorescent protein along with a plasmid encoding FLAG-tagged H2B. After imaging, we approximated the bound-to-free fraction of the frankenbody fusions by calculating the ratio of the intensity of frankenbody fluorescence in the cell nucleus (where FLAG-tagged H2B localizes) to the cytoplasm (where there is presumably very few FLAG tags) (Fig. 1D). This revealed the bound-to-free fraction of the frankenbody is similar when fused with SNAP-tag, HaloTag and mEGFP (p-value > 0.05). Interestingly, fusions to mCherry tended to aggregate (data not shown), whereas fusions to the other red fluorescent protein, mRuby2, actually had the highest bound-to-free fraction (p-value < 0.05). Thus, these data demonstrate the anti-FLAG frankenbody can work when fused to a variety of complementary fluorescent proteins for imaging in up to four colors.

Finally, we wanted to test the binding turnover time of the anti-FLAG frankenbody. For this, we performed fluorescence recovery after photobleaching (FRAP) experiments in living U2OS cells that co-expressed the anti-FLAG FB-mEGFP along with 4×FLAG-mCh-H2B. In these experiments, since H2B has a FRAP recovery time on the order of hours, any fluorescence recovery observed in the frankenbody channel that occurs on the minutes or seconds timescales can be attributed almost

entirely to frankenbody turnover rather than H2B turnover. As shown in Fig, 1E, the FRAP recovery halftime (thalf) of the anti-FLAG frankenbody is 35.3 ± 2.2 s. While this recovery time is considerably faster than that of the anti-HA frankenbody (thalf = 141±7 s) (26), the timescale is longer than other scFv we have developed to image histone modifications (31). Thus, although binding might not be as tight as the anti-HA frankenbody, the more rapid turnover can be advantageous in certain instances; for example, rapid turnover can minimize interference with tagged protein functionality and also minimize photobleaching (since frankenbody photobleached in the imaging plane can unbind and be replaced by a non-photobleached frankenbody).

Signal amplification using the anti-FLAG frankenbody

Before coupling the anti-FLAG frankenbody with ZF proteins for genomic loci visualization, we first wanted to verify it could be used for signal amplification. To test this, we coexpressed anti-FLAG FB-mEGFP along with mito-mCh fused either to a 10×FLAG spaghetti monster tag (mito-mCh-smFLAG) or a 1×FLAG tag (mito-mCh-1×FLAG). To gauge signal amplification, we imaged the two combinations of plasmids under the same conditions and quantified the ratio of background-subtracted GFP to mCherry fluorescence at mitochondria (Fig. 2A). For the mito-mCh-1×FLAG construct, the ratio was 0.032 ± 0.007 (Mean ± SEM; n=30), while for the mito-mCh-smFLAG construct, the ratio was significantly higher at 0.250 ± 0.050 (Mean ± SEM; n=30). Dividing the ratios implies there are on average 7.7 ± 2.2 (Mean ± SEM) more anti-FLAG frankenbodies binding to smFLAG than to 1×FLAG, suggesting significant signal amplification.

To further test the limits of signal amplification, we next used the anti-FLAG frankenbody to track the translation dynamics of single reporter mRNAs using Nascent Chain Tracking (45). For this, we transfected cells with a reporter plasmid encoding 24×MS2 stem loops in the 3'UTR and a 10×smFLAG at the N-terminus of the nuclear protein KDM5B (Fig. 2B). With this reporter, single-mRNA translation sites can be detected by the colocalization of reporter mRNA (labeled by bead-loaded Halo/JF646-tagged MS2 coat proteins) and nascent protein (labeled by co-expressed anti-FLAG FB-mEGFP). As shown in Fig. 2C and 2D, we could indeed detect and track multiple single mRNA translation sites, and each site was sensitive to the addition of the translation inhibitor puromycin. Thus, the anti-FLAG frankenbody can amplify signals from 10×FLAG tags for single molecule tracking experiments.

Design, expression, purification, and evaluation of Zinc-finger DNA-binding protein probes

With the anti-FLAG and anti-HA frankenbodies in hand, we next wanted to couple them with complementary ZF probes to mark and track a pair of genomic loci in living cells in two separate colors. With this goal in mind, we engineered a pair of ZF probes to precisely bind two closely-associated genomic regions in 3D cellular space. In the design process, we followed three guiding principles. First, the ZF target sequence should be within 10 kb from the chromatin contact sites considering the resolution of light microscopy (46, 47). Second, because ZF probes have a strong binding affinity to target DNA, albeit weaker than dCas9 with sgRNA, the ZF target sequence should not overlap the functional binding motifs of common DNA-binding regulators, CpG islands, or any sequence that has the possibility for high DNA methylation. Third, non-existing ZF binding domain

sequence combinations should be avoided, as each ZF domain recognizes 3 bp of DNA and the available target triplet sequences are limited (48).

To choose a model region of chromatin contact sites, we analyzed the GSE104334 data set, which is a HiC contact map of the HCT116-AID system cell line (49). We used HiC-Pro (50) and Juicebox (51) and aligned with HCT116 Hi-C (52), ENCODE HCT116 CTCF ChIP-Seq (ENCSR000BSE), and RNA-Seq (ENCSR000CWM) data (Supplementary Fig. S2). We picked a pair of genomic loci predicted by both algorithms to be in frequent contact on chromosome 8 (Fig. 3A and Supplementary Fig. S2). We used Zinc Finger Tools (37) to generate DNA sequences encoding two ZF probes that bind to the target sequences 600 kb apart. This resulted in a pair of ZF probes, each containing 6 ZF binding domains to recognize 18 bp of unmethylated DNA. Finally, we tagged each ZF probe with either a 10× linear HA or FLAG epitope tag to efficiently recruit anti-HA and FLAG frankenbodies for two-color signal amplification (Fig. 3B).

We next expressed and purified His-tagged ZF probes in E. coli (Supplementary Fig. S3). We evaluated the binding specificity and affinity of the purified ZF probes (ZF-F and ZF-R) using an electrophoretic mobility shift assay and Cy3-labeled double-stranded oligonucleotides. The mobility of oligo-DNA containing the ZF target sequence was shifted in the presence of the corresponding ZF probes, whereas those with a few nucleotide substitutions did not show mobility shifts (Fig. 4A and 4B). These data indicate that the ZF probes selectively bind to the target sequences, as designed. We also estimated the binding affinity of the ZF probes to oligo-DNA, by varying protein concentrations (1-150 nM) with fixed concentrations of oligo-DNA (15 nM) in the assay. The dissociation constant (KD), calculated by the adapted Michaelis-Menten equation, was 42 ± 3 and 41 ± 3 nM (Mean ± SEM) for ZF probes F and R, respectively (Fig. 4C and 4D). These dissociation constants are higher than eukaryotic DNA binding proteins (KD μM level), but lower than typical bacterial repressors (KD pM level) (23, 24) and sgRNA-dCas9 (KD a few nM) (53, 54).

ZF probes were closely associated depending on cohesin in living cells

Having tested the ZF probes in vitro, we next tested their ability to label endogenous DNA in living HCT116-RAD21-mAID-mClover cells (30). In these cells, a cohesin subunit RAD21 gene was replaced with RAD21-mAID-mClover, the degradation of which can be induced by auxin (Fig. 5A). HCT116-RAD21-mAID-mClover cells were transfected with expression plasmids for anti-HA and anti-FLAG frankenbodies (anti-HA mCherry-FB and anti-FLAG iRFP-FB). A few days after transfection, purified ZF probes were added in the medium at a final concentration of 5 μM each for 2 h, during which time the ZF probes were incorporated into cells. Without ZF probes, transiently expressed frankenbodies distributed throughout the nucleus and cytoplasm (Fig. 5B). Although cytoplasmic aggregations were often observed in this cell line particularly under a high laser excitation that is needed to detect weak ZF probe signals, no nuclear foci were formed without ZF probes (Fig. 5B, top). By contrast, in cells incubated with ZF probes, two nuclear foci were observed (Fig. 5B, bottom). Some ZF-F and ZF-R foci were close together (arrowheads) and others were far apart (arrows). The distance of the two nearest probes ranged from 0.6 to 3.7 μm (n=96) (Fig. 5C). As clusters from 0.6-1.2 μm were observed, we set 1.2 μm as a co-association cut-off point to categorize the spot distance

into co- and no-association groups (Fig. 5C). Among 96 pairs, 51 (53.1%) showed co-association of two probes (Fig. 5C). To validate the specificity of the ZF probes, we used a mouse cell line that contained the target sequence to the ZF-F probe, but not the ZF-R probe. In these cells, as expected, ZF-F, but not ZF-R, showed foci in mouse cells that were brightly labeled by frankenbodies (Supplementary Fig. S4A and S4B). Time-lapse imaging revealed that the ZF probe accumulated in foci in the nucleus within 1 h (Supplementary Fig. 4A).

To analyze the contribution of cohesin on the association of the two ZF probes, cohesion degradation was induced by auxin in HCT116-RAD21-mAID-mClover cells (30). After the addition of auxin, the overall RAD21-mClover signal was decreased to 15% in 2 h and further down to 7% in 4 h (Supplementary Fig. S5), confirming that the auxin-induced degradation system was effective as reported (30). Cells expressing frankenbodies were loaded with the ZF probes and fluorescence images were captured every 1 h immediately after auxin addition (Fig. 6A). Pairs of probes that were originally < 1.2 μm apart became substantially more separated in 1 h and afterwards (Fig. 6B). Analysis of 54 pairs of ZF probes revealed that their distances were significantly far apart in 1 h and reached steady state separation in 2 h (Fig. 6B; Supplementary Table S3). These data are consistent with the defect of cohesion induced by RAD21 degradation (49). In control cells without auxin, the distance of the ZF probes remained unchanged for 2 h (Fig. 6C).

We next analyzed the function of CTCF and WAPL (Wings apart-like protein homolog) in the association of ZF probes by knockdown individually and simultaneously using a lentivirus shRNA expression system (Fig. 7A). CTCF is a zinc-finger protein that can be an anchor to define the boundary for CTCF-dependent cohesin (49, 55 and 56) and WAPL regulates cohesin dynamics by disassembling the cohesin ring complex (57-59). Knockdown of both CTCF and WAPL results in loosing chromatin contacts because CTCF depletion disrupts cohesin-anchoring at specific sites and WAPL depletion leads to an extended loop formation with increase in the size of topologically associating domains (60). Immunoblotting showed the levels of CTCF and WAPL were decreased to roughly 17% and 6%, respectively, by single shRNA expression, and 22% and 8%, respectively, by double expression (Fig. 7A). We measured the ZF probe distance in knockdown cells that were still viable under these conditions (Fig. 7B). CTCF knockdown caused the separation of the two ZF probes, but to a lesser degree than RAD21 degradation (Fig. 7C). WAPL knockdown had a milder effect on the probe distance compared to CTCF knockdown (Fig. 7C). The double knockdown of CTCF and WAPL appeared to have an additive effect compared to the single knockdown, causing the separation of the two ZF probes at a similar level to cohesin degradation (Fig. 7C).

Genome organization was partially recovered by cohesion restoration

We finally examined if the separated ZF probes by RAD21 degradation become re-associated by cohesin restoration. HCT116-RAD21-mAID-mClover cells were incubated with auxin for 4 h to degrade RAD21, and then cells were further incubated with a fresh auxin-free medium to restore the cohesin complex. The level of RAD21-mAID-mClover recovered to ~74% (n=107 cells) compared to the control without auxin treatments in 6 h (Supplementary Fig. S6A). Cell viability dropped to ~65% in auxin for 4 h and was restored to ~75% in 6-24 h after washing away auxin (Supplementary Fig. S6B).

To look for signs of ZF probes target loci re-association, we tracked 22 pairs of ZF probes for 12 h (Fig. 8A). Two ZF probe pairs were still associated with a distance <1.2 μm after auxin treatment. The other 20 pairs showed significant distance reduction after 2 h RAD21 recovery (Fig. 8B; Supplementary Fig. S3). Even though 15 pairs with a distance >3.6 μm did not restore their co-association status, 5 pairs with a distance between 1.2 and 3.6 μm dropped below the 1.2 μm association cut-off point after a 6 h recovery (Fig. 8A).

DISCUSSION

In this report, we demonstrated how a pair of ZF probes fused to repeat FLAG and HA epitopes can be coupled with anti-FLAG and anti-HA frankenbodies to mark and track the looping dynamics of two endogenous genomic loci in single living cells. To achieve this, we first created an anti-FLAG frankenbody that complements our recently developed anti-HA frankenbody and that enables the imaging of FLAG-tagged proteins in multiple colors and in diverse live-cell settings. We next designed a pair of synthetic ZF probes that bind uniquely to two endogenous genomic loci that are close to one another in cellular 3D space. The combination of these two imaging systems allowed us to brightly label and track the relative dynamics of the two target genomic loci in single cells over timescales ranging from sub-seconds to hours.

The ZF probe-based technology has several advantages. First, we showed our ZF probes can bind target DNA with high affinity, but not as high as TALEs and dCas9, which stay on DNA for minutes and can interfere with transcription and replication (61-63). The low toxicity of ZF probes has made ZF-based therapies popular in ongoing human clinical trials (64-67). Second, our ZF probes are cell permeable, so we could characterize them biochemically in vitro and later load them into living cells in a controlled manner for optimal experiments. Third, our ZF probes amplify signals at endogenous loci without the need for time-consuming genetic engineering and without requiring a large and permanently attached exogenous tag. While similar systems have been created by amplifying CRISPR-Cas9 signals using the MS2 system (19, 68), the SunTag system (42), or a combination of the two (69), our technology is orthogonal and should therefore enable multiplexed imaging in live cells.

While advantageous in several ways, there are a couple of disadvantages of our ZF probes worth pointing out. First, ZF probe design is target sequence limited. Currently only 49 out of 64 nucleotide triplet combinations are available for targeting (48). Fortunately, this limitation is not very problematic in our case because genome visualization based on light microscopy does not require base-pair resolution. Thus, unlike genome editing, which requires a precise target cut site, target site selection for live-cell imaging can be within a few-kb region, providing a fair amount of flexibility in the ZF design process. Second, our ZF probes tended to aggregate in the cytoplasm of living cells. Fortunately, this did not interfere significantly with our imaging of genomic loci in the cell nucleus. That being said, if a target genomic locus is very close to the nuclear periphery, it may be more difficult to distinguish it from artifactual cytoplasmic aggregates. To circumvent this problem, microscopes with a

good sectioning and/or superresolution system, e.g., confocal or light-sheet microscope, will be helpful (70).

To demonstrate the potential of our ZF probes, we used them to investigate the role of the cohesin complex in genome organization. This required us to design two unique ZF probes to bind to two endogenous genomic loci that are predicted to be in close contact in 3D cellular space. Consistent with these predictions, when we imaged our ZF probe pair with anti-FLAG and anti-HA frankenbodies in living cells, they were associated with each other in bright nuclear loci in more than half of all cells. Time-lapse imaging further revealed that the two loci became separated after triggered RAD21 degradation. Some separated foci were re-associated by cohesin restoration, as previously demonstrated by Hi-C (49). The association rate after cohesin restoration (31.8%; 7 out of 22) was smaller than that in untreated cells (53.1%), suggesting that cohesin-mediated chromatin association is not deterministic. Thus, our work provides strong evidence that our ZF probes are indeed properly localized and that their relative distance can be used to directly visualize cohesin-mediated chromatin loop dynamics in single, living cells. In addition, we also showed data implicating the involvement of CTCF and WAPL in maintaining chromatin structure. CTCF can be an anchor and definer for the cohesion border that provides control over looping activities (49, 55, 56). In line with this, our data directly demonstrates CTCF knockdown leads to the loosening of chromatin contacts, but not to the same degree as RAD21 degradation. These data therefore suggest the existence of a CTCF-independent loop (71, 72). The depletion of WAPL also had a mild but significant impact on chromatin contact and double depletion of CTCF and WAPL had an additive effect, which is consistent with a recent study showing that WAPL depletion resulted in cohesin remaining at CTCF sites (73).

Having demonstrated how to design and use ZF probes to image the dynamics of non-repetitive genomic loci, our technology can now be adapted to image other endogenous genomic loci of interest. In this study we used published Hi-C data to design a pair of ZF probes to study cohesin-mediated chromatin looping (74, 75). Using similar datasets, it is straightforward to design other, similar ZF probes to investigate a wide range of genome dynamics. We therefore anticipate our technology will be of general use to investigate 3D genome dynamics in multiple colors in living cells.

ACKNOWLEDGEMENT

We thank Yuko Sato and Harumi Ueno for cloning anti-FLAG scFv, Takeshi Shimi for instructing the lentivirus expression system, members of Kimura and Stasevich labs for valuable discussion, and the Biomaterials Analysis Division, Open Facility Center, Tokyo Institute of Technology for DNA sequencing.

FUNDING

This work was supported by the Japan Society for the Promotion of Science KAKENHI grant [grant numbers JP18H02170 and JP21H04719 to M.T.K., and JP18H05527 and JP21H04764 to H.K.]; Japan Science and Technology CREST [JPMJCR16G1 to H.K.]; Japan Agency for Medical Research and Development BINDS [JP21am0101105 to H.K.], the National Institutes of Health [R35GM119728

to T.J.S and K99GM141453 to N.Z.] and the National Science Foundation [MCB-1845761 to T.J.S].
Funding for open access charge: Japan Society for the Promotion of Science.

REFERENCES

1. Hansen, A.S., Cattoglio, C., Darzacq, X. and Tjian, R. (2017) Recent evidence that TADs and chromatin loops are dynamic structures. Nucleus, 9, 1–18.
2. Baumann, K. (2020) Human cohesin extrudes interphase DNA to make loops. Nat Rev Mol Cell Bio, 21, 3–3.
3. Dekker, J., Rippe, K., Dekker, M. and Kleckner, N. (2002) Capturing Chromosome Conformation. Science, 295, 1306–1311.
4. Lieberman-Aiden, E., Berkum, N.L. van, Williams, L., Imakaev, M., Ragoczy, T., Telling, A., Amit, I., Lajoie, B.R., Sabo, P.J., Dorschner, M.O., et al. (2009) Comprehensive Mapping of Long-Range Interactions Reveals Folding Principles of the Human Genome. Science, 326, 289–293.
5. Bickmore, W.A. (2012) The Spatial Organization of the Human Genome. Annu Rev Genom Hum G, 14, 67–84.
6. Nora, E.P., Lajoie, B.R., Schulz, E.G., Giorgetti, L., Okamoto, I., Servant, N., Piolot, T., Berkum, N.L. van, Meisig, J., Sedat, J., et al. (2012) Spatial partitioning of the regulatory landscape of the X-inactivation centre. Nature, 485, 381–385.
7. Dixon, J.R., Selvaraj, S., Yue, F., Kim, A., Li, Y., Shen, Y., Hu, M., Liu, J.S. and Ren, B. (2012) Topological domains in mammalian genomes identified by analysis of chromatin interactions. Nature, 485, 376–380.
8. Pombo, A. and Dillon, N. (2015) Three-dimensional genome architecture: players and mechanisms. Nat Rev Mol Cell Bio, 16, 245–257.
9. Wijgerde, M., Grosveld, F. and Fraser, P. (1995) Transcription complex stability and chromatin dynamics in vivo. Nature, 377, 209–213.
10. Dillon, N., Trimborn, T., Strouboulis, J., Fraser, P. and Grosveld, F. (1997) The Effect of Distance on Long-Range Chromatin Interactions. Mol Cell, 1, 131–139.
11. Joyce, E.F., Williams, B.R., Xie, T. and Wu, C.-ting (2012) Identification of Genes That Promote or Antagonize Somatic Homolog Pairing Using a High-Throughput FISH–Based Screen. Plos Genet, 8, e1002667.
12. Gizzi, A.M.C., Cattoni, D.I., Fiche, J.-B., Espinola, S.M., Gurgo, J., Messina, O., Houbron, C., Ogiyama, Y., Papadopoulos, G.L., Cavalli, G., et al. (2019) Microscopy-Based Chromosome Conformation Capture Enables Simultaneous Visualization of Genome Organization and Transcription in Intact Organisms. Mol Cell, 74, 212-222.e5.
13. Woglar, A., Yamaya, K., Roelens, B., Boettiger, A., Köhler, S. and Villeneuve, A.M. (2020) Quantitative cytogenetics reveals molecular stoichiometry and longitudinal organization of meiotic chromosome axes and loops. Plos Biol, 18, e3000817.
14. Shaban, H.A., Barth, R. and Bystricky, K. (2020) Navigating the crowd: visualizing coordination between genome dynamics, structure, and transcription. Genome Biol, 21, 278.

15. Robinett, C.C., Straight, A., Li, G., Willhelm, C., Sudlow, G., Murray, A. and Belmont, A.S. (1996) In vivo localization of DNA sequences and visualization of large-scale chromatin organization using lac operator/repressor recognition. J Cell Biology, 135, 1685–1700.

16. Michaelis, C., Ciosk, R. and Nasmyth, K. (1997) Cohesins: Chromosomal Proteins that Prevent Premature Separation of Sister Chromatids. Cell, 91, 35–45.

17. Lindhout, B.I., Fransz, P., Tessadori, F., Meckel, T., Hooykaas, P.J.J. and Zaal, B.J. van der (2007) Live cell imaging of repetitive DNA sequences via GFP-tagged polydactyl zinc finger proteins. Nucleic Acids Res, 35, e107–e107.

18. Miyanari, Y., Ziegler-Birling, C. and Torres-Padilla, M.-E. (2013) Live visualization of chromatin dynamics with fluorescent TALEs. Nat Struct Mol Biol, 20, 1321–1324.

19. Ma, H., Tu, L.-C., Naseri, A., Chung, Y.-C., Grunwald, D., Zhang, S. and Pederson, T. (2018) CRISPR-Sirius: RNA scaffolds for signal amplification in genome imaging. Nat Methods, 15, 928–931.

20. Anton, T., Bultmann, S., Leonhardt, H. and Markaki, Y. (2014) Visualization of specific DNA sequences in living mouse embryonic stem cells with a programmable fluorescent CRISPR/Cas system. Nucleus, 5, 163–172.

21. Chen, B., Gilbert, L.A., Cimini, B.A., Schnitzbauer, J., Zhang, W., Li, G.-W., Park, J., Blackburn, E.H., Weissman, J.S., Qi, L.S., et al. (2013) Dynamic Imaging of Genomic Loci in Living Human Cells by an Optimized CRISPR/Cas System. Cell, 155, 1479–1491.

22. Ran, F.A., Hsu, P.D., Wright, J., Agarwala, V., Scott, D.A. and Zhang, F. (2013) Genome engineering using the CRISPR-Cas9 system. Nat Protoc, 8, 2281–2308.

23. Isalan, M., Choo, Y. and Klug, A. (1997) Synergy between adjacent zinc fingers in sequence-specific DNA recognition. Proc National Acad Sci, 94, 5617–5621.

24. Imanishi, M., Hori, Y., Nagaoka, M. and Sugiura, Y. (2000) DNA-Bending Finger: Artificial Design of 6-Zinc Finger Peptides with Polyglycine Linker and Induction of DNA Bending †. Biochemistry-us, 39, 4383–4390.

25. Saad, H., Gallardo, F., Dalvai, M., Tanguy-le-Gac, N., Lane, D. and Bystricky, K. (2014) DNA Dynamics during Early Double-Strand Break Processing Revealed by Non-Intrusive Imaging of Living Cells. Plos Genet, 10, e1004187.

26. Zhao, N., Kamijo, K., Fox, P.D., Oda, H., Morisaki, T., Sato, Y., Kimura, H. and Stasevich, T.J. (2019) A genetically encoded probe for imaging nascent and mature HA-tagged proteins in vivo. Nat Commun, 10, 2947.

27. Choo, Y., Sánchez-García, I. and Klug, A. (1994) In vivo repression by a site-specific DNA-binding protein designed against an oncogenic sequence. Nature, 372, 642–645.

28. Barrow, J.J., Masannat, J. and Bungert, J. (2012) Neutralizing the function of a β-globin–associated cis-regulatory DNA element using an artificial zinc finger DNA-binding domain. Proc National Acad Sci, 109, 17948–17953.

29. Gaj, T., Liu, J., Anderson, K.E., Sirk, S.J. and Barbas, C.F. (2014) Protein Delivery Using Cys2–His2 Zinc-Finger Domains. Acs Chem Biol, 9, 1662–1667.

30. Natsume, T., Kiyomitsu, T., Saga, Y. and Kanemaki, M.T. (2016) Rapid Protein Depletion in Human Cells by Auxin-Inducible Degron Tagging with Short Homology Donors. Cell Reports, 15, 210–218.

31. Sato, Y., Mukai, M., Ueda, J., Muraki, M., Stasevich, T.J., Horikoshi, N., Kujirai, T., Kita, H., Kimura, T., Hira, S., et al. (2013) Genetically encoded system to track histone modification in vivo. Sci Rep-uk, 3, 2436.

32. Cialek, C.A., Galindo, G., Koch, A.L., Saxton, M.N. and Stasevich, T.J. (2021) Bead Loading Proteins and Nucleic Acids into Adherent Human Cells. J Vis Exp, 10.3791/62559.

33. Grimm, J.B., English, B.P., Chen, J., Slaughter, J.P., Zhang, Z., Revyakin, A., Patel, R., Macklin, J.J., Normanno, D., Singer, R.H., et al. (2015) A general method to improve fluorophores for live-cell and single-molecule microscopy. Nat Methods, 12, 244–250.

34. Koulouras, G., Panagopoulos, A., Rapsomaniki, M.A., Giakoumakis, N.N., Taraviras, S. and Lygerou, Z. (2018) EasyFRAP-web: a web-based tool for the analysis of fluorescence recovery after photobleaching data. Nucleic Acids Res, 46, gky508-.

35. Tokunaga, M., Imamoto, N. and Sakata-Sogawa, K. (2008) Highly inclined thin illumination enables clear single-molecule imaging in cells. Nat Methods, 5, 159–161.

36. Waldo, G.S., Standish, B.M., Berendzen, J. and Terwilliger, T.C. (1999) Rapid protein-folding assay using green fluorescent protein. Nat Biotechnol, 17, 691–695.

37. Mandell, J.G. and Barbas, C.F. (2006) Zinc Finger Tools: custom DNA-binding domains for transcription factors and nucleases. Nucleic Acids Res, 34, W516–W523.

38. Rueden, C.T., Schindelin, J., Hiner, M.C., DeZonia, B.E., Walter, A.E., Arena, E.T. and Eliceiri, K.W. (2017) ImageJ2: ImageJ for the next generation of scientific image data. Bmc Bioinformatics, 18, 529.

39. Yang, X., Boehm, J.S., Yang, X., Salehi-Ashtiani, K., Hao, T., Shen, Y., Lubonja, R., Thomas, S.R., Alkan, O., Bhimdi, T., et al. (2011) A public genome-scale lentiviral expression library of human ORFs. Nat Methods, 8, 659–661.

40. Ewert, S., Honegger, A. and Plückthun, A. (2004) Stability improvement of antibodies for extracellular and intracellular applications: CDR grafting to stable frameworks and structure-based framework engineering. Methods, 34, 184–199.

41. Sato, Y., Kujirai, T., Arai, R., Asakawa, H., Ohtsuki, C., Horikoshi, N., Yamagata, K., Ueda, J., Nagase, T., Haraguchi, T., et al. (2016) A Genetically Encoded Probe for Live-Cell Imaging of H4K20 Monomethylation. J Mol Biol, 428, 3885–3902.

42. Tanenbaum, M.E., Gilbert, L.A., Qi, L.S., Weissman, J.S. and Vale, R.D. (2014) A Protein-Tagging System for Signal Amplification in Gene Expression and Fluorescence Imaging. Cell, 159, 635–646.

43. Wongso, D., Dong, J., Ueda, H. and Kitaguchi, T. (2017) Flashbody: A Next Generation Fluobody with Fluorescence Intensity Enhanced by Antigen Binding. Anal Chem, 89, 6719–6725.

44. Colca, J.R., McDonald, W.G., Waldon, D.J., Leone, J.W., Lull, J.M., Bannow, C.A., Lund, E.T. and Mathews, W.R. (2004) Identification of a novel mitochondrial protein (“mitoNEET”) cross-linked specifically by a thiazolidinedione photoprobe. Am J Physiol-endoc M, 286, E252–E260.

45. Morisaki, T., Lyon, K., DeLuca, K.F., DeLuca, J.G., English, B.P., Zhang, Z., Lavis, L.D., Grimm, J.B., Viswanathan, S., Looger, L.L., et al. (2016) Real-time quantification of single RNA translation dynamics in living cells. Science, 352, 1425–1429.

46. Brandão, H.B., Gabriele, M. and Hansen, A.S. (2021) Tracking and interpreting long-range chromatin interactions with super-resolution live-cell imaging. Curr Opin Cell Biol, 70, 18–26.

47. Banigan, E.J., Berg, A.A. van den, Brandão, H.B., Marko, J.F. and Mirny, L.A. (2020) Chromosome organization by one-sided and two-sided loop extrusion. Elife, 9, e53558.

48. Durai, S., Mani, M., Kandavelou, K., Wu, J., Porteus, M.H. and Chandrasegaran, S. (2005) Zinc finger nucleases: custom-designed molecular scissors for genome engineering of plant and mammalian cells. Nucleic Acids Res, 33, 5978–5990.

49. Rao, S.S.P., Huang, S.-C., Hilaire, B.G.S., Engreitz, J.M., Perez, E.M., Kieffer-Kwon, K.-R., Sanborn, A.L., Johnstone, S.E., Bascom, G.D., Bochkov, I.D., et al. (2017) Cohesin Loss Eliminates All Loop Domains. Cell, 171, 305-320.e24.

50. Servant, N., Varoquaux, N., Lajoie, B.R., Viara, E., Chen, C.-J., Vert, J.-P., Heard, E., Dekker, J. and Barillot, E. (2015) HiC-Pro: an optimized and flexible pipeline for Hi-C data processing. Genome Biol, 16, 259.

51. Robinson, J.T., Turner, D., Durand, N.C., Thorvaldsdóttir, H., Mesirov, J.P. and Aiden, E.L. (2018) Juicebox.js Provides a Cloud-Based Visualization System for Hi-C Data. Cell Syst, 6, 256-258.e1.

52. Li, G., Ruan, X., Auerbach, R.K., Sandhu, K.S., Zheng, M., Wang, P., Poh, H.M., Goh, Y., Lim, J., Zhang, J., et al. (2012) Extensive Promoter-Centered Chromatin Interactions Provide a Topological Basis for Transcription Regulation. Cell, 148, 84–98.

53. Sternberg, S.H., Redding, S., Jinek, M., Greene, E.C., Doudna, J.A. (2014) DNA interrogation by the CRISPR RNA-guided endonuclease Cas9. Nature, 507, 62–67.

54. Cencic, R., Miura, H., Malina, A., Robert, F., Ethier, S., Schmeing, T.M., Dostie, J., Pelletier, J. (2014) Protospacer Adjacent Motif (PAM)-Distal Sequences Engage CRISPR Cas9 DNA Target Cleavage. PLoS ONE, 9, e109213.

55. Parelho, V., Hadjur, S., Spivakov, M., Leleu, M., Sauer, S., Gregson, H.C., Jarmuz, A., Canzonetta, C., Webster, Z., Nesterova, T., et al. (2008) Cohesins Functionally Associate with CTCF on Mammalian Chromosome Arms. Cell, 132, 422–433.

56. de Wit, E., Vos, E.S.M., Holwerda, S.J.B., Valdes-Quezada, C., Verstegen, M.J.A.M., Teunissen, H., Splinter, E., Wijchers, P.J., Krijger, P.H.L. and de Laat, W. (2015) CTCF Binding Polarity Determines Chromatin Looping. Mol Cell, 60, 676–684.

57. Gerlich, D., Koch, B., Dupeux, F., Peters, J.-M. and Ellenberg, J. (2006) Live-Cell Imaging Reveals a Stable Cohesin-Chromatin Interaction after but Not before DNA Replication. Curr Biol, 16, 1571–1578.

58. Kueng, S., Hegemann, B., Peters, B.H., Lipp, J.J., Schleiffer, A., Mechtler, K. and Peters, J.-M. (2006) Wapl Controls the Dynamic Association of Cohesin with Chromatin. Cell, 127, 955–967.

59. Tedeschi, A., Wutz, G., Huet, S., Jaritz, M., Wuensche, A., Schirghuber, E., Davidson, I.F., Tang, W., Cisneros, D.A., Bhaskara, V., et al. (2013) Wapl is an essential regulator of chromatin structure and chromosome segregation. Nature, 501, 564–568.

60. Wutz, G., Várnai, C., Nagasaka, K., Cisneros, D.A., Stocsits, R.R., Tang, W., Schoenfelder, S., Jessberger, G., Muhar, M., Hossain, M.J. et al. (2017) Topologically associating domains and chromatin loops depend on cohesin and are regulated by CTCF, WAPL, and PDS5 proteins. EMBO J. 36, 3573-3599.

61. Jiang, F., Zhou, K., Ma, L., Gressel, S. and Doudna, J.A. (2015) A Cas9–guide RNA complex preorganized for target DNA recognition. Science, 348, 1477–1481.

62. Garcia-Bloj, B., Moses, C., Sgro, A., Plani-Lam, J., Arooj, M., Duffy, C., Thiruvengadam, S., Sorolla, A., Rashwan, R., Mancera, R.L., et al. (2016) Waking up dormant tumor suppressor genes with zinc fingers, TALEs and the CRISPR/dCas9 system. Oncotarget, 7, 60535–60554.

63. Rinaldi, F.C., Doyle, L.A., Stoddard, B.L. and Bogdanove, A.J. (2017) The effect of increasing numbers of repeats on TAL effector DNA binding specificity. Nucleic Acids Res, 45, gkx342-.

64. Perez, E.E., Wang, J., Miller, J.C., Jouvenot, Y., Kim, K.A., Liu, O., Wang, N., Lee, G., Bartsevich, V.V., Lee, Y.-L., et al. (2008) Establishment of HIV-1 resistance in CD4+ T cells by genome editing using zinc-finger nucleases. Nat Biotechnol, 26, 808–816.

65. Wilen, C.B., Wang, J., Tilton, J.C., Miller, J.C., Kim, K.A., Rebar, E.J., Sherrill-Mix, S.A., Patro, S.C., Secreto, A.J., Jordan, A.P.O., et al. (2011) Engineering HIV-Resistant Human CD4+ T Cells with CXCR4-Specific Zinc-Finger Nucleases. Plos Pathog, 7, e1002020.

66. Tebas, P., Stein, D., Tang, W.W., Frank, I., Wang, S.Q., Lee, G., Spratt, S.K., Surosky, R.T., Giedlin, M.A., Nichol, G., et al. (2014) Gene Editing of CCR5 in Autologous CD4 T Cells of Persons Infected with HIV. New Engl J Medicine, 370, 901–910.

67. Lee, H.B., Sundberg, B.N., Sigafoos, A.N. and Clark, K.J. (2016) Genome Engineering with TALE and CRISPR Systems in Neuroscience. Frontiers Genetics, 7, 47.

68. Qin, P., Parlak, M., Kuscu, C., Bandaria, J., Mir, M., Szlachta, K., Singh, R., Darzacq, X., Yildiz, A. and Adli, M. (2017) Live cell imaging of low- and non-repetitive chromosome loci using CRISPR-Cas9. Nat Commun, 8, 14725.

69. Hong, Y., Lu, G., Duan, J., Liu, W. and Zhang, Y. (2018) Comparison and optimization of CRISPR/dCas9/gRNA genome-labeling systems for live cell imaging. Genome Biol, 19, 39.

70. Boettiger, A. and Murphy, S. (2020) Advances in Chromatin Imaging at Kilobase-Scale Resolution. Trends Genet, 36, 273–287.

71. Schmidt, D., Schwalie, P.C., Ross-Innes, C.S., Hurtado, A., Brown, G.D., Carroll, J.S., Flicek, P. and Odom, D.T. (2010) A CTCF-independent role for cohesin in tissue-specific transcription. Genome Res, 20, 578–588.

72. Hansen, A.S., Hsieh, T.-H.S., Cattoglio, C., Pustova, I., Saldaña-Meyer, R., Reinberg, D., Darzacq, X. and Tjian, R. (2019) Distinct Classes of Chromatin Loops Revealed by Deletion of an RNA-Binding Region in CTCF. Mol Cell, 76, 395-411.e13.

73. Liu, N.Q., Maresca, M., Brand, T. van den, Braccioli, L., Schijns, M.M.G.A., Teunissen, H., Bruneau, B.G., Nora, E.P. and Wit, E. de (2021) WAPL maintains a cohesin loading cycle to preserve cell-type-specific distal gene regulation. Nat Genet, 53, 100–109.

74. Sati, S. and Cavalli, G. (2017) Chromosome conformation capture technologies and their impact in understanding genome function. Chromosoma, 126, 33–44.

75. Szabo, Q., Bantignies, F. and Cavalli, G. (2019) Principles of genome folding into topologically associating domains. Sci Adv, 5, eaaw1668.

FIGURES LEGENDS

Fig. 1. Development of an anti-FLAG frankenbody to label FLAG-tagged proteins in living cells.
(A) A schematic showing how to design anti-FLAG frankenbodies (anti-FLAG-FB) using anti-FLAG-scFv CDRs and stable scFv scaffolds. (B) Representative cells showing the respective localization of the anti-FLAG frankenbody in living U2OS cells co-expressing FLAG-tagged proteins of interest (POIs), including nuclear protein histone H2B (n=20 cells), cytoplasmic protein β-actin (n=9 cells) and mitochondria (n=30 cells), with the FLAG tag located at either the N- or C- terminus (anti-FLAG frankenbody, green; FLAG-tagged mCh-POIs, magenta). (C) Normalized fluorescence intensity plots of the yellow dashed lines shown in (B) for both frankenbody (green) and FLAG-tagged mCh-POI channels (magenta). (D) Upper panel: Representative cell images of anti-FLAG frankenbody fused to multiple fluorescent fusion proteins (GFP, mRuby2, SNAP-tag/JF646 and HaloTag/JF646) and specifically labeleling FLAG-tagged nuclear protein H2B (FLAG-tagged H2B). Lower panel: Box plot showing the nuclear to cytoplasmic fluorescence intensity ratio (Nuc/Cyt) for all cells imaged in upper panel; 21 cells in one independent experiment for each fluorophore. (E) Left: Plot of the anti-FLAG and anti-HA frankenbody FRAP data with fitted curves for representative cells (the green solid line is the FRAP recovery curve for the anti-FLAG frankenbody and the gray solid line is the fitted curve; the green dashed line is the FRAP recovery curve for the anti-HA frankenbody and gray dashed line is the fitted curve); Right: Box plot showing the recovery halftimes of all FRAP experiments for the anti-FLAG frankenbody (n=23 cells in 2 independent experiments) and the anti-HA frankenbody. Fits from 23 cells reveal the mean FRAP recovery halftime (thalf) of the anti-FLAG frankenbody is 35.3±2.2 s (cell-to-cell SEM), while that of the anti-HA frankenbody is 141±7 s. Scale bars: 10 μm. For box plots, the center lines show the medians; the boxes indicate 25-75%; whiskers extend 1.5 times the interquartile range from the 25th and 75th percentiles.

Fig. 2. Amplifying fluorescence with the anti-FLAG frankenbody.
(A) Left: Representative cells expressing the anti-FLAG frankenbody (green) labeling mitochondria with 1× or 10×FLAG (smFLAG) tags (magenta); Right: Box plot of the fluorescence intensity ratio of the anti-FLAG FB-GFP labeling Mito-mCh-1×FLAG or -10×FLAG (smFLAG). The ratio is 0.032±0.007 (Mean ± SEM) for 1×FLAG (n=30 cells) and 0.250±0.050 (Mean ± SEM) for 10×FLAG (n=30 cells),

indicating, on average, 7.7±2.2 (Mean ± SEM) anti-FLAG FB-GFP bind to 10×FLAG (smFLAG). (B) A diagram depicting frankenbody (anti-FLAG FB-GFP; green) and MCP-HaloTag/JF646 (magenta) labeling FLAG epitopes and mRNA MS2 stem loops, respectively, in a KDM5B translation reporter. (C) A representative cell showing the colocalization of anti-FLAG FB-GFP (green) with KDM5B mRNA (magenta). (D) A montage of the representative translation spot highlighted in b showing the disappearance of nascent chain signals within seconds of adding the translational inhibitor puromycin. (E) The normalized number of mRNA spots (magenta) and nascent chain spots (green) as a function of time after adding the translational inhibitor puromycin (n=9 cells in 3 independent experiments, error bars show the cell-to-cell SEM). Scale bars, 10 μm. For box plots, center lines show the medians; the boxes indicate 25-75%; whiskers extend 1.5 times the interquartile range from the 25th and 75th percentiles.

Fig. 3. Designing a pair of zinc-finger protein probes to track chromatin contact sites.
(A) Chromatin contact sites predicted by different HiC algorithms are chosen. (B) A schematic of a DNA-bound ZF probe that contains 6 DNA recognition domains and 10× HA or FLAG linear epitopes for signal amplification upon binding of complementary fluorescent frankenbodies. (C) A schematic of chromatin looping and unlooping. Two ZF probes that bind to the sites of chromatin contact are expected to be observed within a close distance of one another (DC; the probe distance in the presence of a loop). When cohesin is absent, the two probes will be more separated (DL; the probe distance in the absence of a loop).

Fig. 4. Binding specificity and affinity of ZF probes.
Binding of ZF probes with DNA was analyzed by a gel mobility shift assay. (A and B) Double stranded Cy3-labeled DNA (20 nM) was mixed with ZF probes F (A) and R (B) (6.25, 12.5, 25, 50, and 100 nM for DNA containing the target sequence; and 100 nM for control DNA). Oligonucleotide sequences and the mutation sites (in red) are indicated. ZF probes bound specifically to the target sequence. (C and D) Double stranded Cy3-labeled DNA containing the target sequence (20 nM) was mixed with ZF probes F (C) and R (D) (1-150 nM). The binding affinity (dissociation constant; KD) was calculated based on the curve of bound fractions of DNA with respect to the ZF probe concentration.

Fig. 5. Visualizing genomic foci using ZF probes and frankenbodies in living cells.
(A) A flow chart of the genome visualization method. Cells are transfected with expression vectors of anti-HA mCherry-frankenbody (FB) and anti-FLAG iRFP-FB and then incubated with the HA- and Flag-tagged ZF probes, which are incorporated into cells. (B) Representative single confocal sections of living HCT116-RAD21-mAID-GFP cells that express frankenbodies without (-) and with (+) incubation with ZF probes. Frankenbodies are seen in the cytoplasm without ZF probes, but two nuclear foci in the nucleus (arrowheads and arrows) were only observed after incubation of cells with ZF probes F (magenta) and R (green). In the nucleus with ZF probes, one pair of probes were located close together (arrowheads) and another pair were far apart (arrows). (C) Distance between the nearest ZF probes F and R. The distances of all pairs are plotted in the middle. As there is a gap at a separation distance of ~1.2 μm and separation distances as large as 3.5 μm were observed, a

threshold was set at 1.2 μm to classify probe pairs into two groups with co-association (53%; 51 out of 96) or no association (47%; 45 out of 96). Scale bar, 5 μm.

Fig. 6. Dissociation of genomic loci induced by cohesin degradation.
HCT116-mAID-RAD21-mClover cells were transfected with anti-FLAG and anti-HA frankenbody expression vectors, loaded with ZF probes, and were treated (A and B) or untreated (C) with auxin. (A) Representative confocal images of living HCT116-RAD21-mAID-mClover cells loaded with ZF probe F (mCherry frankenbody; red) and R (iRFP frankenbody; green). The nuclear foci of ZF probes F and R were closely associated 5 min after addition of auxin (red and green arrowheads), but became separated in 30 min (magenta and green arrows). Nuclear areas are indicated in dashed line in merged images. Scale bar, 5 μm. (B) Box plot of the distance between ZF probes F and R, which were originally associated before auxin addition, at the indicated time point after auxin addition (n=54 ZF probe pairs). The statistical analysis was performed between 5 min and 1 h and 2 h (others not tested) by Wilcoxon signed-rank test (*** $p < 0.001$; see Supplementary Table S3). (C) Box plot of the distance between ZF probes F and R in mock treated cells without auxin (n=12). There is no significant difference between the different time points by Wilcoxon signed-rank test. For box plots, center lines show the medians; the boxes indicate 25-75%; whiskers extend 1.5 times the interquartile range from the 25th and 75th percentiles.

Fig. 7. Effects of CTCF and WAPL knockdown (KD) on the association of ZF probe target loci.
CTCF and WAPL in HCT116-RAD21-mAID-mClover cells were independently and simultaneously knocked down by lentivirus-mediated shRNA expression. (A) Immunoblotting of CTCF and WAPL in KD cells. (B) Confocal images of ZF probes F (mCherry; magenta) and R (iRFP; green) in KD cells. Arrows and arrowheads indicate the separate and associated foci, respectively. Scale bar, 5 μm. (C) Box plot of ZF probe distance in CTCF-KD (n=54), WAPL-KD (n=54) and CTCF and WAPL double KD cells (n=17). The significance was analyzed by Wilcoxon signed-rank test (*** $p<0.001$). For box plots, center lines show the medians; the boxes indicate 25-75%; whiskers extend 1.5 times the interquartile range from the 25th and 75th percentiles.

Fig. 8. Reassociation of ZF probe target loci by RAD21 restoration.
HCT116-RAD21-mAID-mClover cells were transfected with anti-FLAG and anti-HA frankenbody expression vectors, loaded with ZF probes, and treated with auxin for 4 h to degrade RAD21. After washing away auxin, cells were placed on a confocal microscope and further incubated with auxin-free medium to measure the distance between the two ZF probes. (A) Distances of 22 pairs of ZF probes during 12-h RAD21 recovery. (B) Box plot of ZF probe distance during RAD21 recovery. For box plots, center lines show the medians; the boxes indicate 25-75%; whiskers extend 1.5 times the interquartile range from the 25th and 75th percentiles. The statistical analysis by Wilcoxon signed-rank test indicated a significant difference between 0 and 2 h (*** $p < 0.001$; see Supplementary Table S4).

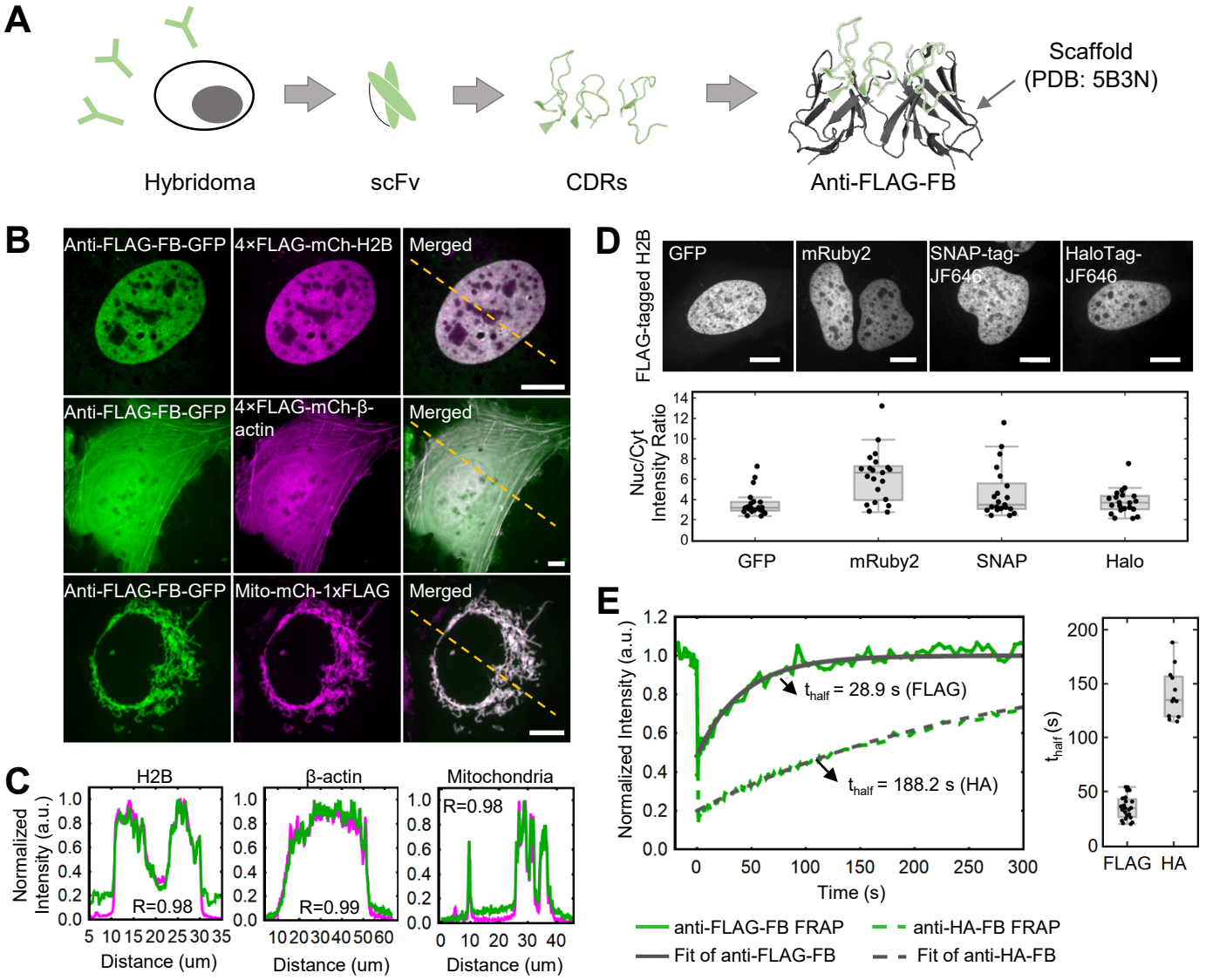

Fig. 1. Development of an anti-FLAG frankenbody to label FLAG-tagged proteins in living cells. (**A**) A cartoon schematic showing how to design anti-FLAG frankenbody (anti-FLAG-FB) using anti-FLAG-scFv CDRs and stable scFv scaffolds. (**B**) Representative cells showing the respective localization of the anti-FLAG frankenbody in living U2OS cells co-expressing FLAG-tagged nuclear protein histone H2B (n=20 cells), cytoplasm protein β-actin (n=9 cells) and mitochondria (n=30 cells) with the FLAG tag located at either N- or C- terminus (anti-FLAG frankenbody, green; FLAG tagged mCh-POIs, magenta). (**C**) Normalized fluorescence intensity plot of the yellow dash lines shown in (**B**) for both frankenbody(green) and FLAG tagged mCh-POI channels (magenta). (**D**) Upper panel: Representative cell images of anti-FLAG frankenbody fused to multiple fluorescent fusion proteins (GFP, mRuby2, SNAP-tag/JF646 and HaloTag/JF646) specifically labels FLAG-tagged nuclear protein H2B (FLAG-tagged H2B). Lower panel: Nuclear to cytoplasmic fluorescence intensity ratio (Nuc/Cyt) plots for all cells imaged in (**C**) upper panel; 21 cells in one independent experiment for each fluorophore. (**E**) Left: Plot of the anti-FLAG and anti-HA frankenbody FRAP data with fitted curves for representative cells (green solid line is the actual FRAP curve and gray solids line is the fitted curve for anti-FLAG frankenbody; green dashed line is the actual FRAP curve and gray dashed line is the fitted curve for anti-HA frankenbody); Right: Half recovery time plot of FRAP experiments for anti-FLAG frankenbody (n=23 cells in 2 independent experiments) and anti-HA frankenbody. Fits from 23 cells reveal the FRAP mean half recovery time of the anti-FLAG frankenbody, t_{half}, is 35.3 ± 2.2 sec (cell-to-cell SEM). Scale bars: 10 μm. For box plots, center lines show the medians; the boxes indicate 25-75%; whiskers extend 1.5 times the interquartile range from the 25th and 75th percentiles; and data points are plotted.

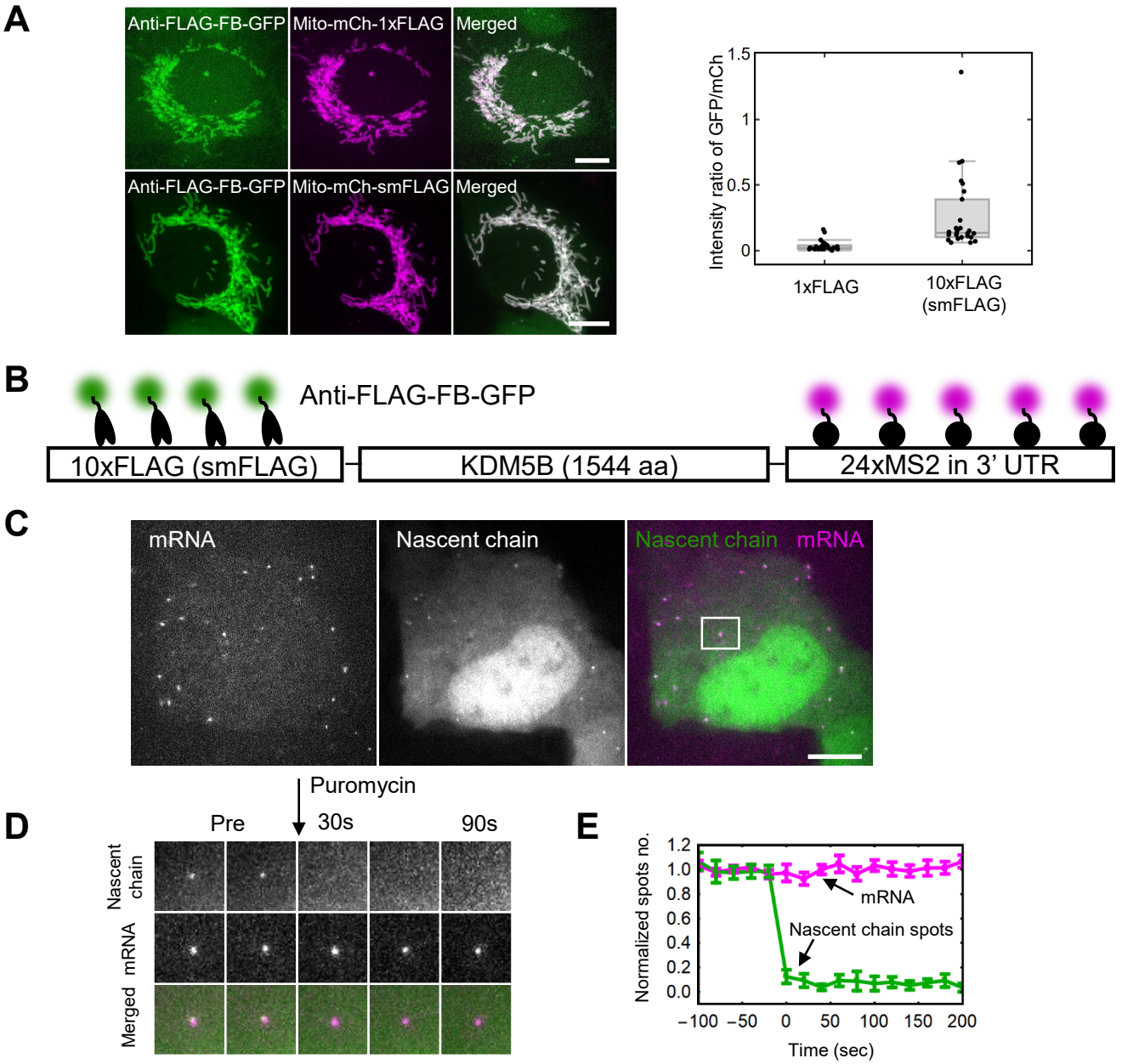

Fig. 2. Amplifying protein and mRNA translation fluorescence with the anti-FLAG frankenbody. (**A**) Left: Representative cells of anti-FLAG frankenbody (green) labeling Mitochondria with 1x or 10xFLAG (smFLAG) tag (magenta); Right: Plot of fluorescence intensity ratio of anti-FLAG-FB-GFP to Mito-mCh-1x or -10xFLAG (smFLAG). The ratio is 0.032 ± 0.007 (Mean ± SEM) for 1xFLAG (n=30 cells) and 0.250 ± 0.050 (Mean ± SEM) for 10xFLAG (n=30 cells), indicating, in average, 7.7 ± 2.2 (Mean ± SEM) anti-FLAG-FB-GFP binds to 10xFLAG (smFLAG). (**B**) A diagram depicting frankenbody (anti-FLAG-FB-GFP; green) and MCP-HaloTag/JF646 (magenta) labeling FLAG epitopes and mRNA stem loops, respectively, in a KDM5B translation reporter. (**C**) A representative cell showing colocalization of anti-FLAG-FB-GFP (green) with KDM5B mRNA (magenta). (**D**) A representative translation spot (highlighted in b) montage showing the disappearance of nascent chain spots within seconds after adding a translational inhibitor puromycin. (**E**) Normalized mRNA spots (magenta) and nascent chain spots numbers (green) change with time before and after adding a translation inhibitor puromycin (n=9 cells in 3 independent experiments, error bar is cell-to-cell SEM). Scale bars, 10 μm. For box plots, center lines show the medians; the boxes indicate 25-75%; whiskers extend 1.5 times the interquartile range from the 25th and 75th percentiles; and data points are plotted.

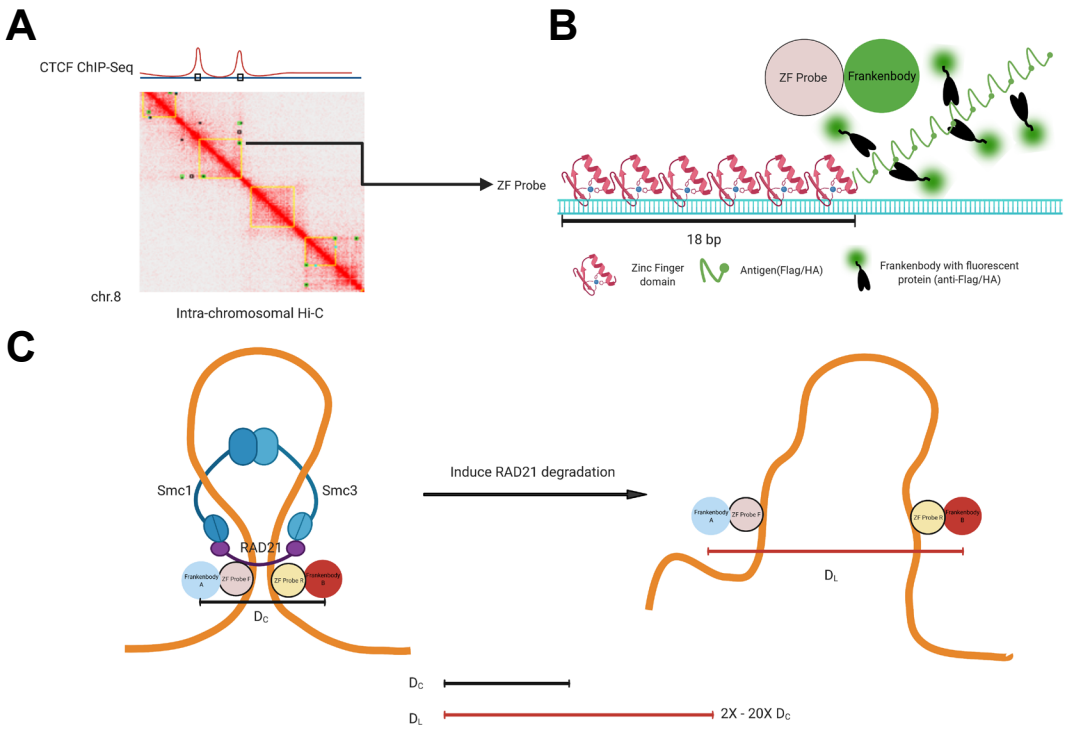

Fig. 3. Designing a pair of zinc-finger protein probes to track chromatin contact.
(**A**) Chromatin contact sites predicted by different HiC algorithms are chosen. (**B**) A schematic illustration for DNA-bound ZF probe that contains 6 DNA reorganization domains and 10X HA or Flag linear epitopes for multiple binding of the fluorescent protein-tagged frankenbody. (**C**) A schematic illustration of chromatin looping and unlooping. Two ZF probes that bind to the sites of chromatin contact are expected to be observed with a close distance (D_C; the probe distance in cohesion status) in the presence of cohesin complex. When cohesin is absent, the two probes will be separately detected (D_L; the probe distance in loose status).

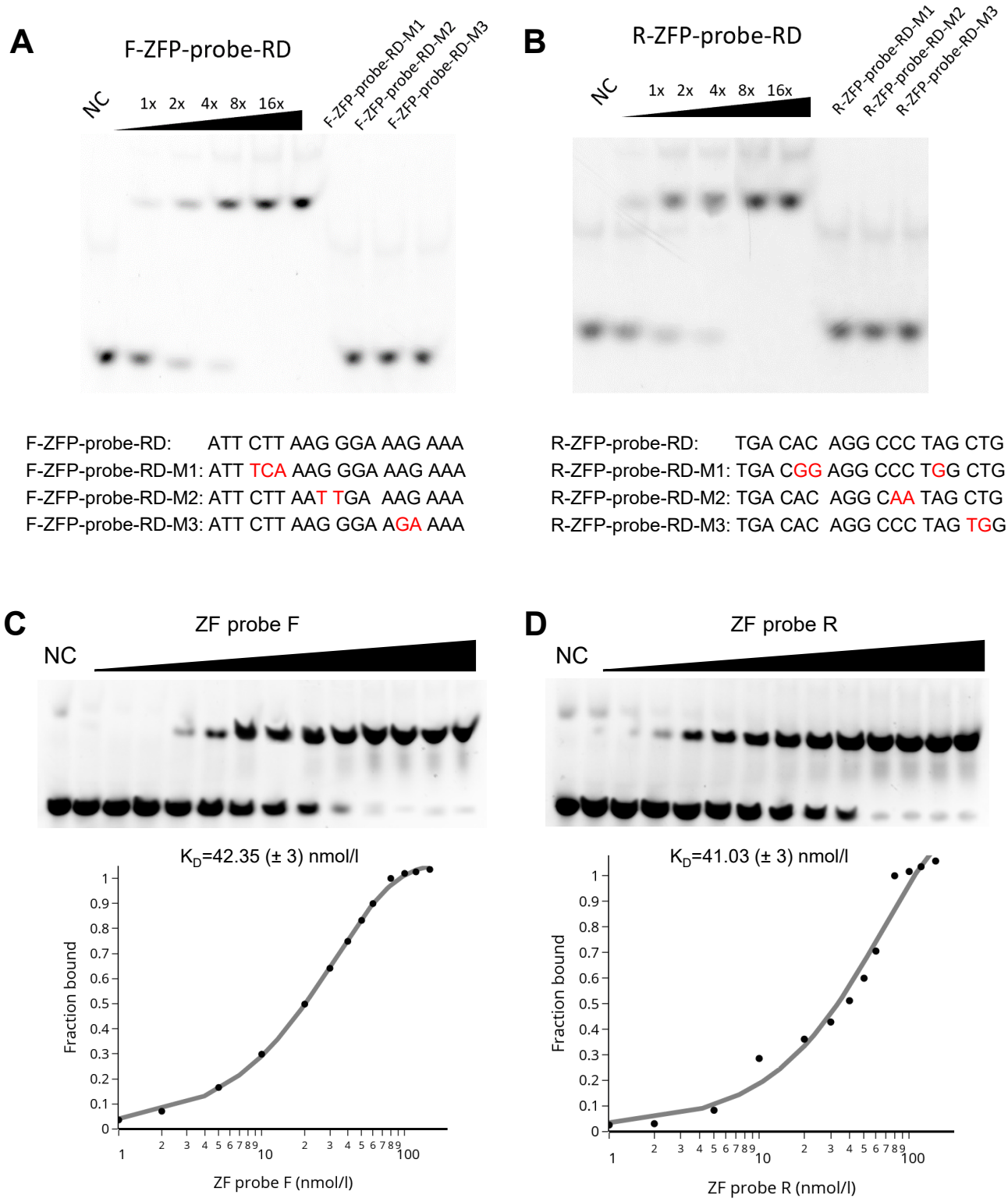

Fig. 4. Binding specificity and affinity ZF probes.
Binding of ZF probes with DNA was analyzed by gel retardation assay. (**A** and **B**) Double stranded Cy3-labeled DNA (20 nM) was mixed with ZF probes F (**A**) and R (**B**) (6.25, 12.5, 25, 50, and 100 nM for DNA containing the target sequence; and 100 nM for control DNA). Oligonucleotide sequence and the mutation sites (in Red) are indicated. ZF probes bound specifically to the target sequence. (**C** and **D**) Double stranded Cy3-labeled DNA containing the target sequence (20 nM) was mixed with ZF probes F (**C**) and R (**D**) (1-150 nM). The binding affinity (dissociation constant; K_D) was calculated based on the curve of bound fractions of DNA with respect to the ZF probe concentration.

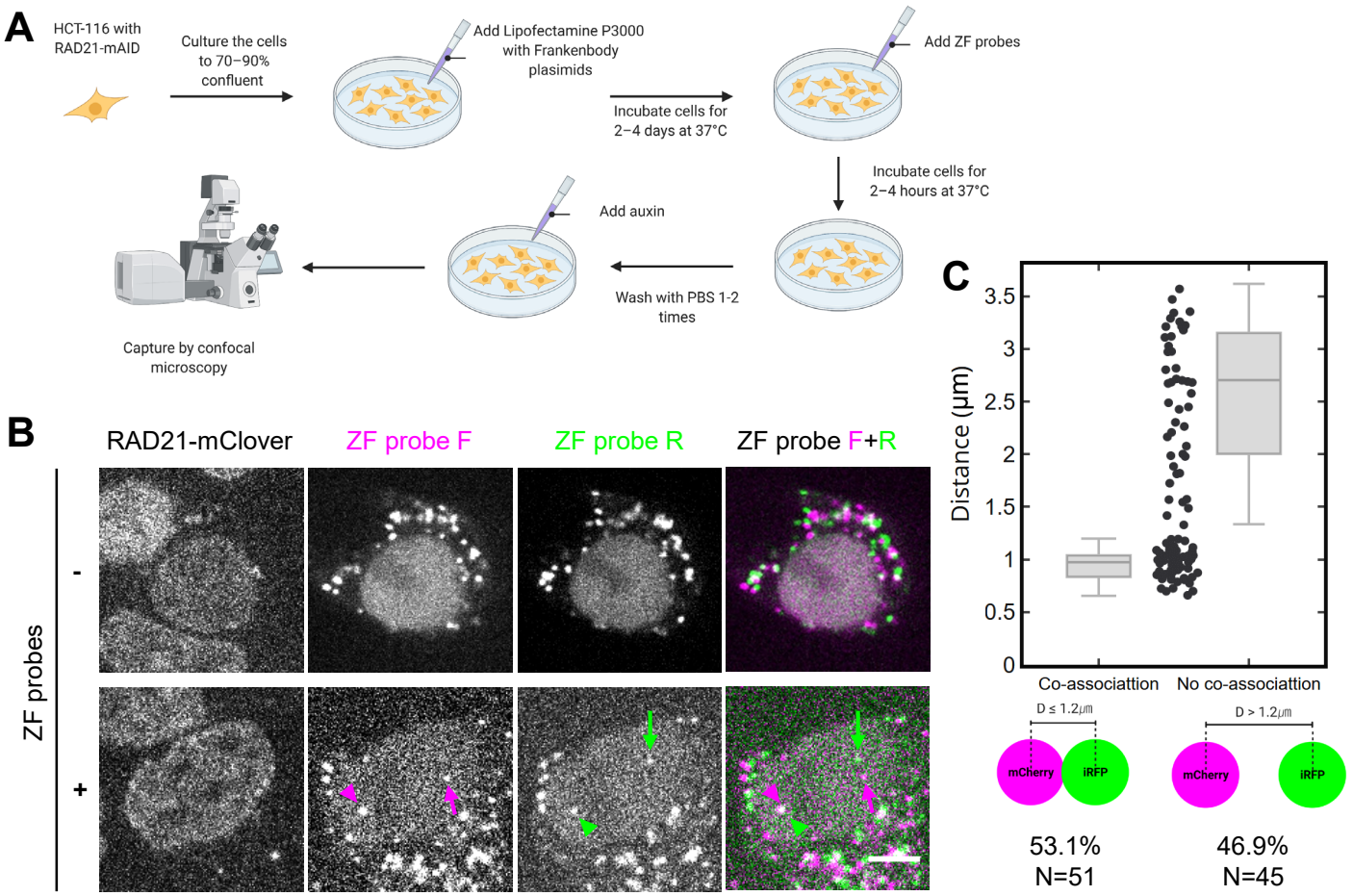

Fig. 5. Visualizing genomic foci using ZF probes and Frankenbodies in living cells.
(**A**) A flow chart of the genome visualization method. Cells are transfected with expression vectors of anti-HA-mCherry and anti-FLAG-iRFP Frankenbodies and then incubated with the HA- and Flag-tagged ZF probes, which are incorporated into cells. (**B**) Representative single confocal sections of living HCT116-RAD21-mAID-GFP cells that express frankenbodies without (-) and with (+) incubation with ZF probes. Frankenbodies are seen in the cytoplasm without ZF probes, but two nuclear foci in the nucleus (arrowheads and arrows) were only observed after incubation of cells with ZF probes F (magenta) and R (green). In the nucleus with ZF probes, two different probes were located close together (arrowheads) and separately (arrows). (**C**) Distance between the nearest ZF probes F and R. The distances of all pairs are plotted in the middle. As there is a gap at 1.2 μm distance between a cluster <1.2 μm and scattered points up to 3.5 μm, a threshold was set at 1.2 μm to classify the groups with co-association (53%; 51 out of 96) and no association (47%; 45 out of 96). Scale bar, 5 μm.

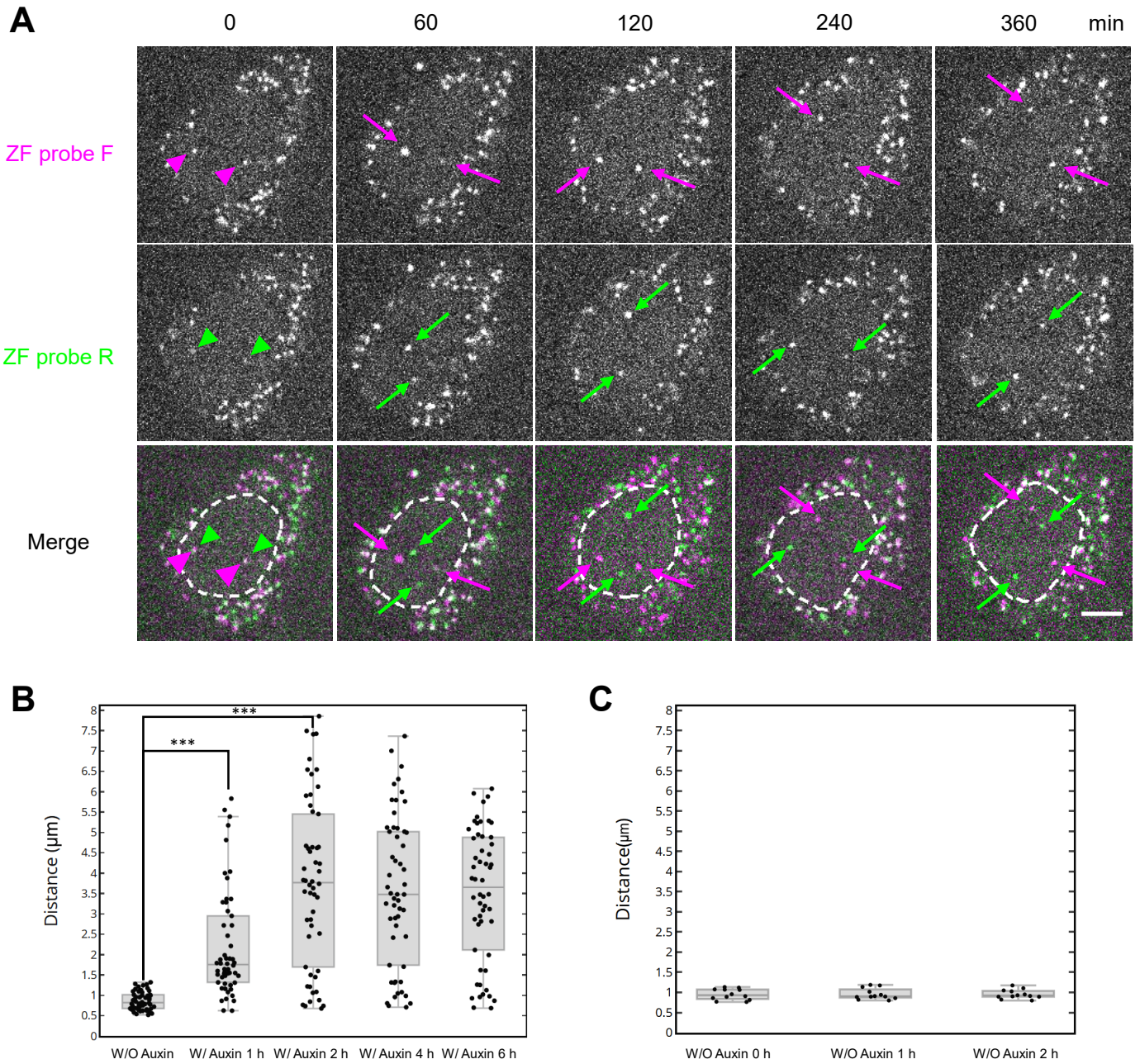

Fig. 6. Dissociation of genomic loci induced by cohesin degradation.
HCT116-mAID-RAD21-mClover cells were transfected with anti-FLAG and anti-HA frankenbody expression vectors, loaded with ZF probes, and were treated (**A** and **B**) or untreated (**C**) with auxin. (**A**) Representative confocal images of living HCT116-RAD21-mAID-mClover cells loaded with ZF probe F (mCherry frankenbody; red) and R (iRFP frankenbody; green). The nuclear foci of ZF probes F and R were closely associated 5 min after addition of auxin (red and green arrowheads), but became separated in 30 min (magenta and green arrows). Nuclear areas are indicated in dashed line in merged images. Scale bar, 5 μm. (**B**) Box plot of the distance between ZF probes F and R, which were originally associated before auxin addition, at the indicated time point after auxin addition (n=54 ZF probe pairs). The statistical analysis was performed between 5 min and 1 h and 2 h (others not tested) by Wilcoxon signed-rank test (*** $p < 0.001$; see Supplementary Table S3). (**C**) Box plot of the distance between ZF probes F and R in mock treated cells without auxin (n=12). There is no significant difference between the different time points by Wilcoxon signed-rank test. For box plots, center lines show the medians; the boxes indicate 25-75%; whiskers extend 1.5 times the interquartile range from the 25th and 75th percentiles.

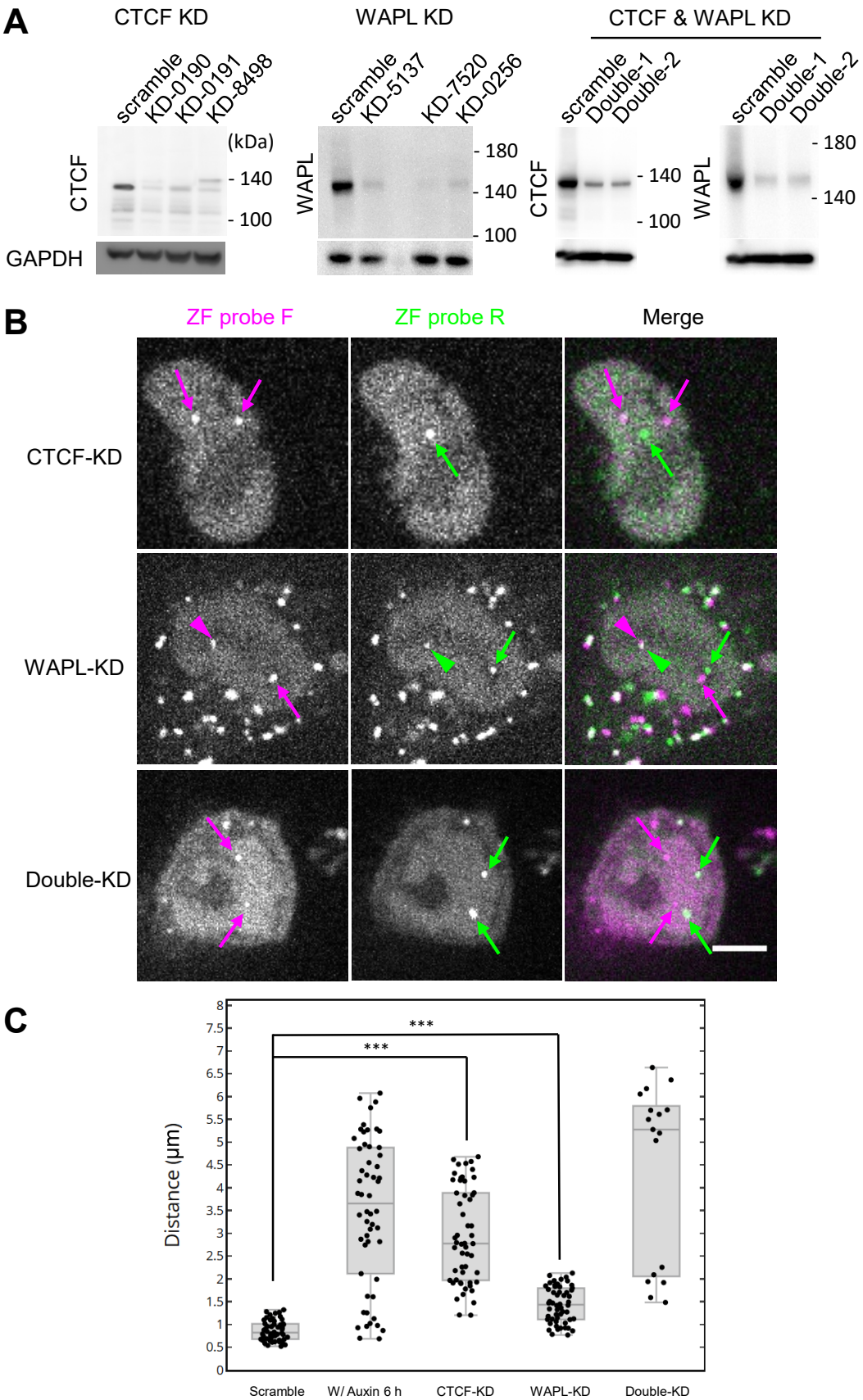

Fig. 7. Effects of CTCF and WAPL knockdown (KD) on the association of two ZF probe target loci. CTCF and WAPL in HCT116-RAD21-mAID-mClover cells were independently and simultaneously knocked down by lentivirus-mediated shRNA expression. (**A**) Immunoblotting of CTCF and WAPL in KD cells. (**B**) Confocal images of ZF probes F (mCherry; magenta) and R (iRPF; green) in KD cells. Arrows and arrowheads indicate the separate and associated foci, respectively. Scale bar, 5 μm. (**C**) Box plot of ZF probe distance in CTCF-KD (n=54), WAPL-KD (n=54) and CTCF and WAPL double KD cells (n=17). The significance was analyzed by Wilcoxon signed-rank test (*** $p<0.001$). For box plots, center lines show the medians; the boxes indicate 25-75%; whiskers extend 1.5 times the interquartile range from the 25th and 75th percentiles; and data points are plotted.

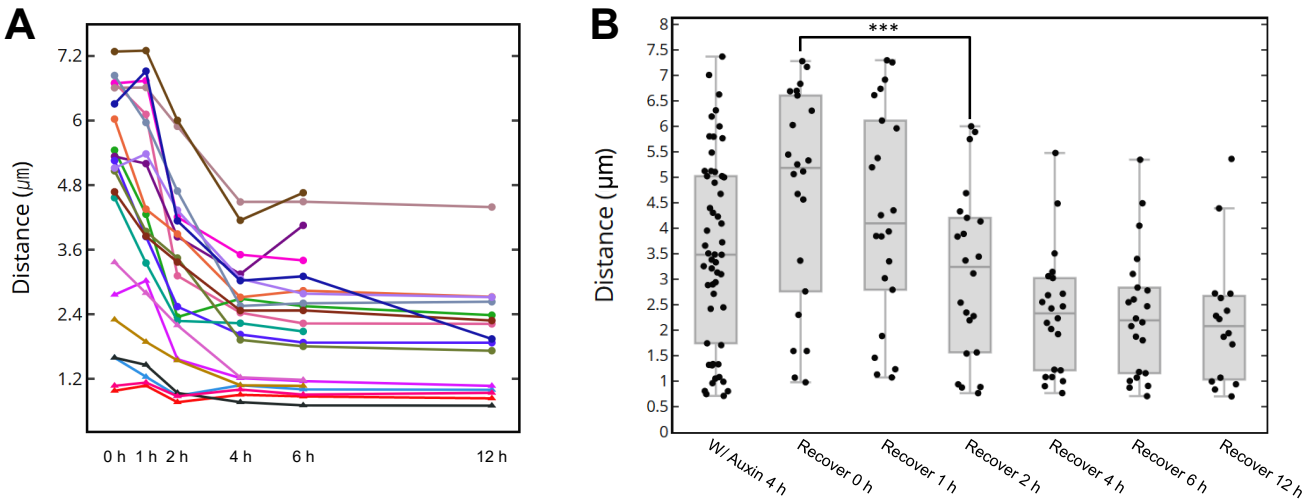

Fig. 8. Reassociation of ZF probe target loci by RAD21 restoration.
HCT116-RAD21-mAID-mClover cells were transfected with anti-FLAG and anti-HA frankenbody expression vectors, loaded with ZF probes, and treated with auxin for 4 h to degrade RAD21. After washing away auxin, cells were set on to a confocal microscope and further incubated with auxin-free medium to measure the distance between the two ZF probes. (**A**) Distances of 22 pairs of ZF probes during 12-h RAD21 recovery. (**B**) Box plot of ZF probe distance during RAD21 recovery. For box plots, center lines show the medians; the boxes indicate 25-75%; whiskers extend 1.5 times the interquartile range from the 25th and 75th percentiles; and data points are plotted. The statistical analysis by Wilcoxon signed-rank test indicated a significant difference between 0 and 2 h (*** $p < 0.001$; see Supplementary Table S4).